CDF/ANAL/EXOTIC/CDFR/10184
Version 2.0
June 28, 2010

Improving WH Neural Network Analysis Using Looser Isolated Tracks

Yoshikazu Nagai[5], Timo Aaltonen[9], Adrian Buzatu[7], Jay Dittmann[1], Martin Frank[1], Richard Hughes[2], Justin Keung[8], Shinhong Kim[5], Ben Kilminster[6], Nils Krumnack[1], Kevin Lannon[2], Christopher Neu[10], Jason Slaunwhite[2], Anyes Taffard[3], Evelyn Thomson[8], Andreas Warburton[7], Brian Winer[2], Homer Wolfe[2], Weiming Yao[4]

[1] *Baylor University*
[2] *Ohio State University*
[3] *UC Irvine*
[4] *LBNL*
[5] *University of Tsukuba*
[6] *FNAL*
[7] *McGill University*
[8] *University of Pennsylvania*
[9] *University of Helsinki*
[10] *University of Virginia*

Abstract

We present a new selection of W events to be used in the $WH \to l\nu b\bar{b}$ analysis. The new events are selected by requiring an isolated track with significant deposits of energy in the calorimeter that are primary from the decay of $W \to e\nu$ or $\tau\nu$ where the electron failed the standard electron selection or the τ decays into a single charged hadron (one-prong). We search for $WH \to l\nu b\bar{b}$ candidate events with two jets, large $\not\!\!E_T$, and exactly one looser isolated track lepton candidate from the missing energy trigger. We present the analysis technique used for these new events, as well as the resulting gain in the acceptance of WH events. This new analysis selection is applied to the data through period 28, corresponding to an integrated luminosity of 5.7 fb^{-1}.

1 Introduction

This note describes an improvement to the existing search for $p\bar{p} \to WH \to \ell\nu b\bar{b}$ in events that have at least one SECVTX b-tagged jet. The improvement consists of

including an additional looser isolated track category to the standard W selection by requiring an isolated track with significant deposits of energy in the calorimeter. In the existing analysis, the lepton was required to be identified as either an electron (CEM, PHX), a muon(CMUP, CMX), or an isolated track with an energy deposit in the calorimeters consistent with that of a minimum-ionizing particle. These new events are selected from the missing energy trigger and are primary from the decay of $W \rightarrow e\nu$ or $\tau\nu$ where the electron failed the standard electron selection or the τ decays into a single charged hadron (one-prong). Treating this new lepton type as an independent channel, we go through the full analysis procedure,including b-tagging, forming an event discriminant, and setting limits on the WH production cross section. These limits will be used in combination with the full $WH \rightarrow l\nu b\bar{b}$ analysis, as well as with other channels.

2 Data Samples and Event Selection

The data used for this analysis come from the $\not\!\!E_T$ dataset (`emet`), which were collected through Feb. 2010. We select events with no tight leptons reconstructed, but containing a high-p_T isolated track that are required to pass one of the following MET triggers:

- `MET35_&_TWO_JETS`
- `MET35_&_CJET_&_JET`
- `MET35_&_CJET_&_JET_LUMI_190`
- `MET35_&_CJET_&_JET_DPS`
- `MET45(MET40)`

We use a $\not\!\!E_T$ + jets (MET2J) and $\not\!\!E_T$ trigger (MET45) parallel and will describe details in the event selection section.

Our Higgs signal model comes from the official Higgs Discovery Group Higgs Monte Carlo (MC) samples generated with Pythia using the standard MC procedure outlined in CDF software version 6.1.4. These Higgs samples were generated for a range of Higgs masses from 100 GeV to 150 GeV. Our background models are composed of a number of components. The W and Z plus light-flavor and heavy-flavor jet processes are modeled using Alpgen version 2.10 showered with Pythia. Likewise, the single-top contribution is modeled using parton-level events generated by MadEvent and showered through Pythia. The rest of the background processes, including the $t\bar{t}$, WW, WZ, and ZZ processes were generated with Pythia. For backgrounds involving a top quark, the top mass was set to 172.5 GeV/c^2.

2.1 Luminosity

We use the standard luminosity calculation provided by the top group including corrections for trigger prescales on a run-section by run-section basis. This calculation uses version 34 of the DQM silicon good run list (bits [1,1,4,1]) for data through period 28. The luminosity for the MET2J triggered events is 5.22 fb^{-1}. The luminosity for the MET45 triggered events is 5.55 fb^{-1}.

2.2 Event Selection

We improve the isolated track selections of the existing $WH \rightarrow l\nu b\bar{b}$ analysis [1] to select additional $W \rightarrow e\nu$ or $W \rightarrow \tau\nu$ events from the$\not\!\!E_T$ triggers where the electron failed the standard electron identification or the τ decays into a single charged hadron (one-prong). We use the same selection criteria outline in Table 1 to select high quality, high-p_T isolated tracks (ISOTKh) with $|\eta_{track}| < 1.2$ and a significant energy deposit in the calorimeter as a tight jet. We define the proximity of our tracks to other activity in the event using track isolation. Track isolation uses only track information and no calorimeter information. It is defined as:

$$\text{TrkIsol} = \frac{p_T(\text{candidate})}{p_T(\text{candidate}) + \sum p_T(\text{trk})}, \tag{1}$$

where $\sum p_T(\text{trk})$ is the sum of the p_T of tracks that meet the following requirements:

- $p_T > 0.5$ GeV
- $\Delta R(\text{trk, candidate}) < 0.4$
- $\Delta Z(\text{trk, candidate}) < 5$ cm
- Number of COT axial hits > 20
- Number of COT stereo hits > 16

Using this definition, a track with no surrounding activity has a isolation of 1.0. This analysis requires track isolation > 0.9, or 90% of the local track p_T. However, the purity of these events is still quite low as shown in the Figure 1 when comparing the corresponding isolation in the hadronic calorimeter (Hadiso) and the minimum $\Delta\phi$ between the$\not\!\!E_T$ and jets in the data and the WH115 Monte Carlo. We use a variety of vetoes that ensure that isolated tracks events are from W events and that they do not overlap other lepton identifications.

- **Two Track Veto**: We count the number of isolated tracks in the event. If there are two or more isolated tracks, we veto the event.
- **Extra Z removal**: We remove the events if any of two opposit-signed high p_T tracks has an invariant mass within the Z mass window between 76 and 106 GeV/c^2.

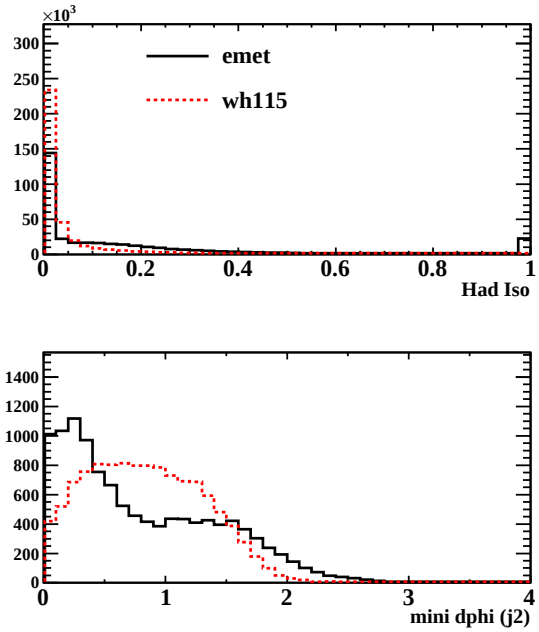

Figure 1: Comparison of the hadronic isolation and the minimum $\Delta\phi$ between $\not\!\!E_T$ and jets for isolated track candidates from the $\not\!\!E_T$ trigger data and the WH115 MC.

- **Standard Lepton and Isolated Track Veto**: If the event contains any identified lepton or an isolated muon-like track (ISOTKm) that used in the standard WH analysis, the event is not allowed to pass the ISOTKh selection.
- **Hadronic Isolation<0.1**: The track is required to be isolated in the hadronic calorimeter (Hadiso) to be consistent with an electron or one-prong hadronic τ decay where the Hadiso is defined as the ratio of sum of energy deposits in the surrounding towers in the hadronic calorimeter over the track p_T.
- $\not\!\!E_T$ **not pointing to any jet**: The $\not\!\!E_T$ is required to not point to any jet $\Delta R > 0.4$.

The $\not\!\!E_T$ is corrected for the presence of muons (including muon-like isolated tracks) and jet energy corrections (JES). The jets are identified using the JetClu algorithm with a cone of 0.4 and are required to be central ($|\eta_{Det.}| < 2.0$) with $E_T > 20$ GeV, corrected for level-5 jet corrections. A cut of $m_T^W > 10$ GeV is required for the 0-tag and single-tagged events to suppress the non-W background contribution.

Jets Trigger Requirements The MET2J trigger has been used extensively at CDF and has shown that that the trigger's jet requirements are fully efficient after the following cuts:

- Two Tight Jets with $E_T > 25$ GeV

Variable	Cut
p_T	> 20 GeV
$\|z_0\|$	< 60 cm
$\|d_0\|$corr	< 0.2
$\|d_0\|$corr (w/SI)	< 0.02
track isolation	> 0.9
Axial COT hits	≥ 24
Stereo Hits	≥ 20
χ^2 probability (data only)	$> 10^{-8}$
Num Si Hits (data only, only if num expect ≥ 3)	≥ 3
Matching to a jet	$\Delta R < 0.4$

Table 1: Looser Isolated track selection cuts

- $\Delta R > 1.0$
- One central jet with $|\eta| < 0.9$

We apply these additional jet cuts after identifying the tight jets in the event. For jet bins ≥ 3, we require that the two lead jets in the event satisfy these requirements. If any one of the MET2J trigger-related requirements above failed, we consider that event as part of an orthogonal sample which requires the MET45 trigger. As a result, we have two exclusive IsoTrk categories, which are referred to as the MET2J and MET45 trigger samples.

We use the parameterization of the MET2J and MET45 trigger turn-on curves for each trigger level separately as a function of level-5 jet corrected vertex $\not\!\!E_T$ that measured using the inclusive CMUP trigger [2]. We choose level-5 jet corrected vertex $\not\!\!E_T$, which is corrected for the primary vertex position and takes into account the level-5 jet energy correction but not corrections derived from muons.

2.3 *b*-Tagging

We adopt the *b*-tagging strategy that used in the standard WH analysis [1], which maximizes the number of events with two or more *b*-tags by making use of the SECVTX, jet probability (5%), and RomaNN algorithms. Every event with at least one SECVTX *b*-tagged jet falls into one of four exclusive tag categories, defined below:

SECVTX **tight + SECVTX tight (ST+ST):** Events in this category are required to have both jets tagged by the tight operating point of SECVTX.

SECVTX **tight + Jet Probability 5% (ST+JP):** Events in this category are required to have one jet tagged by the tight operating point of SECVTX and one jet to be tagged by the jet probability algorithm. To be tagged, a jet must have a jet probability of less than 5%.

SECVTX **tight + RomaNN (ST+RomaNN):** Events in this category are required to have one jet tagged by the tight operating point of SECVTX and one jet to be tagged by the RomaNN algorithm. To be tagged, a jet must have an output value greater than 0.0.

SECVTX **tight:** Events in this category are required to have exact one SECVTX tight tagged jet and with no additional SECVTX, jet probability or RomaNN tags.

In order to further improve the b-tagging purity for the events containing only one SECVTX b-tagged jet, we also include the Karlsruhe Neural Network b-tagger (Kitnn) as a b-jet discriminant from light flavor or charm quarks which uses jet characteristics as well as secondary vertex information [3].

2.4 Neural Network b-jet Energy Correction

The most sensitive variable for WH analysis is the dijet invariant mass. Improvement on dijet mass resolution directly results in improvement of the final sensitivity. To further improve the dijet mass resolution, a neural network based b-jet energy correction method was developed [4]. We employ four neural network functions for each b-tagging type: SECVTX, JP, RomaNN, and not-tagged.

2.5 Neural Network Discriminant

To further improve signal-to-background discrimination after event selection, we employ a Bayesian neural network (BNN) [5] trained on a variety of kinematic variables to distinguish WH from backgrounds. One advantage using BNN is less prone overtraining because of the bayesian sampling.

For this analysis, we use the same BNN discriminant functions that are optimized for the central lepton and one of three tagging categories: ST+ST, ST+JP and ST+RomaNN, and 1-ST [1].

3 Background Estimate

We use the same methodology of background estimation in the lepton-triggered analysis, which is commonly referred to as "Method II" [6].

The W+ jets contribution includes jets from b and c quarks, and light-flavor jets mistagged by the b-tagging algorithm. The effect of true W + heavy-flavor production is estimated from a combination of data and simulation. We use both low and high luminosity ALPGEN Monte Carlo samples to calculate the rate of $Wb\bar{b}, Wc\bar{c}$, and Wc production relative to inclusive W + jets production. Then this relative rate is applied to the observed W + jets sample, after non-W and $t\bar{t}$ contributions have been subtracted. Finally, we apply b-tagging efficiencies and b-tagging scale factors to estimate the background after tagging.

Theoretical Cross Sections	
WW	11.66 ± 0.70 pb
WZ	3.46 ± 0.30 pb
ZZ	1.51 ± 0.20 pb
Single Top s-channel	1.05 ± 0.07 pb
Single Top t-channel	2.10 ± 0.19 pb
$Z +$ jets	787.4 ± 85.0 pb
$t\bar{t}$	7.04 ± 0.6 pb

Table 2: Theoretical cross sections and errors for the electroweak and single top backgrounds, along with the theoretical cross section for $t\bar{t}$.

Contributions from events with falsely tagged light-flavor jets (mistags) are estimated using the latest version of the mistag matrices [7] for SecVtx, JP, and RomaNN b-tagging algorithms.

The normalization of the diboson, $t\bar{t}$ and single top backgrounds are based on the theoretical cross sections (listed in Table 2). The event acceptance and b-tagging efficiency are derived from MC. The acceptance is corrected in MC events for lepton identification, trigger efficiencies and z vertex cut, and b-tagging scale factors.

The signature of W decay can also be mimicked by non-W multijet events which may contain a high-energy reconstructed lepton and missing transverse energy. These can arise from semileptonic heavy-flavor decay or from false reconstructions. The reconstructed leptons from such events are rarely isolated from the rest of the event, as required by our event selection. We therefore calculate the number of non-W events in our selected sample by extrapolating from non-isolated Hadiso sideband region into the signal region.

3.1 Non-W (QCD fake) background

We estimate the non-W fraction in the pretag and tagged samples by fitting the data Hadiso distribution to background templates. The non-W distribution is obtained from the non-isolated (iso > 0.1) loose muon (CMU, CMP, BMU) events. The MC signal template contains events from Z+jet, W+LF, top, and electroweak backgrounds. In order to check the Hadiso modeling, we select the events containing one tight central lepton and one isolated track. The opposite-sign pair with back-to-back provides a clean sample of DY that can compare directly to the Monte Carlo shape. The same-sign pair provides an alternative sample of fakes from the W+jets. The comparison is shown in Figure 2 that the Hadiso modeling seems reasonable.

We use the same uncertainty estimates as described in "Method II For You" [6], which was determined by performing fits with an alternative shape, a variety of binnings and fit ranges. The relative uncertainty on the non-W normalization is 40%. Figures 3 and 4 show the results fitting the Hadiso distribution in the pretag and tag regions.

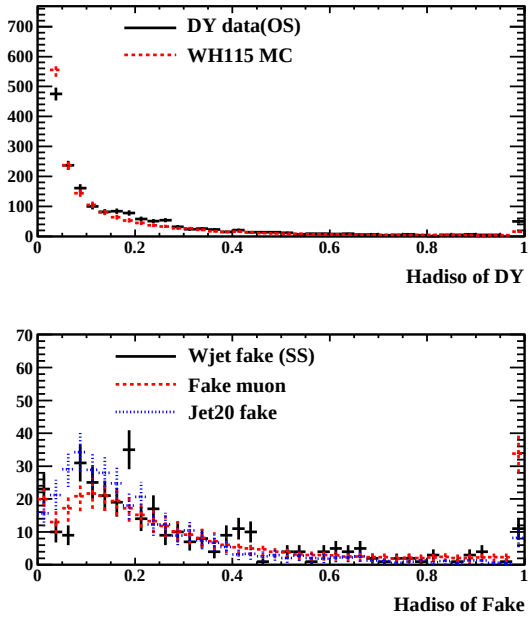

Figure 2: The comparison of hadiso for the signal and the background.

The fits in the double tagged region suffers from low statistics. The uncertainty of 40% accomodates the low statistics.

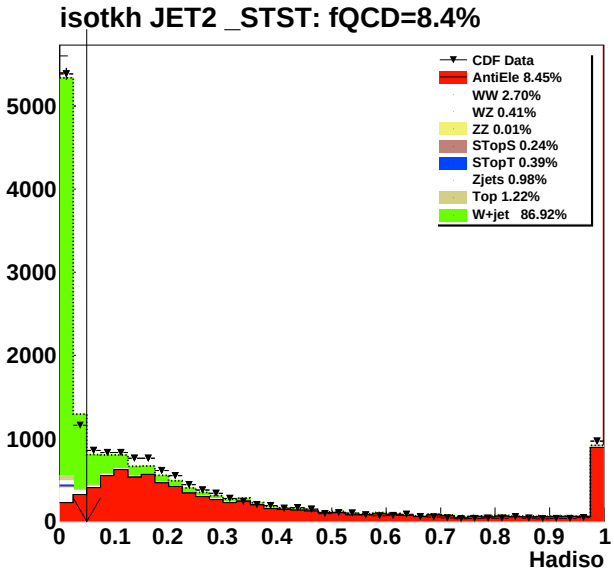

Figure 3: QCD fraction estimate for pretag of the W + 2 jets events.

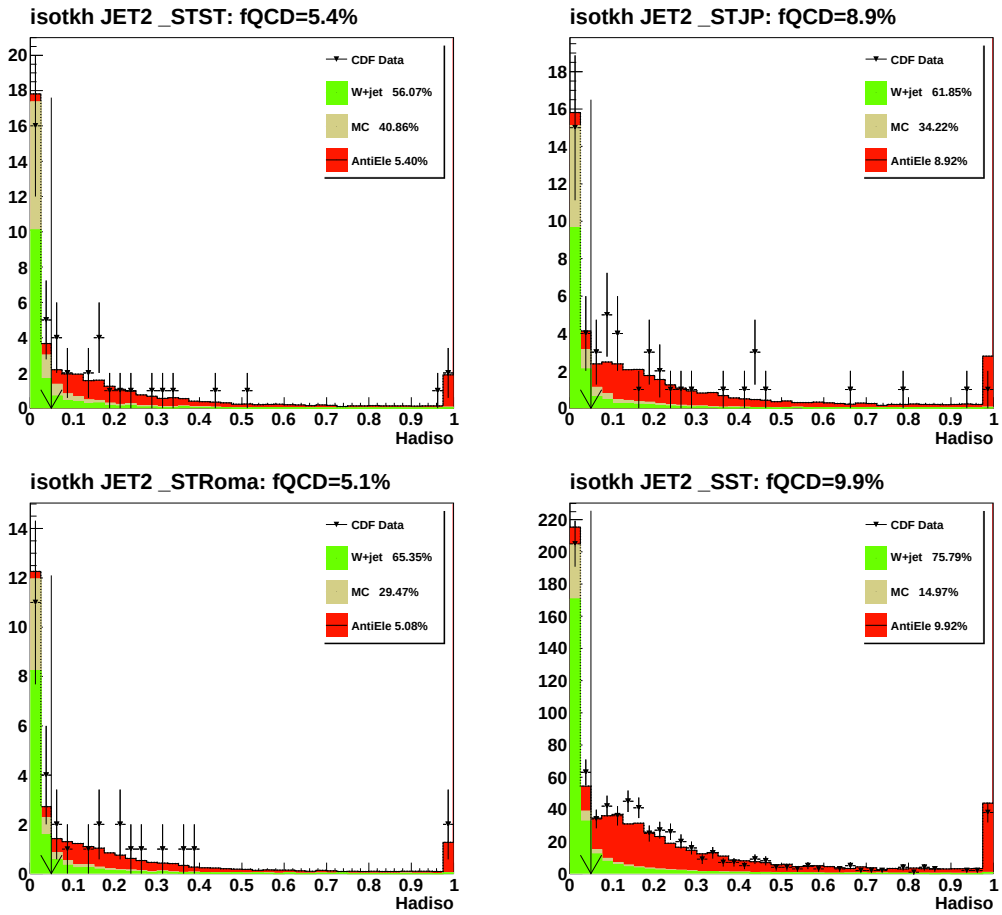

Figure 4: QCD fraction estimate for each b-tagging category (STST, STJP, STRoma, SST) in the W + 2 jets events.

3.2 Background Summary

We have described the contributions of individual background sources to the final background estimate. The summary of the background estimates is shown in Tables 3 - 6 and the number of expected events with observed data as function of jet multiplicity plots are shown in Figures 5 - 8. In general, the number of expected events and the number of observed events are in good agreement.

Sources	1jet	2jet	3jet	4jet	≥5jet
Pretag Events	32488	6544	1145	235	44
W + LF	69.1±12.8	76.7±13.8	16.2±3.27	2.07±0.64	0.23±0.16
W + bb	34.9±10.8	68.3±21.1	19.1±5.98	3.15±1.07	0.41±0.19
W + cc	19.7±6.26	43±13.6	12.9±4.11	2.48±0.86	0.39±0.18
W + cj	33.9±10.7	42.2±13.4	7.66±2.44	1.13±0.39	0.14±0.07
t#bart (7.4 pb)	3.44±0.55	25.8±3.81	38.8±5.56	27.2±3.77	7.64±1.05
Single Top S	1.07±0.17	4.94±0.71	1.33±0.19	0.24±0.03	0.05±0.01
Single Top T	2.02±0.35	9.6±1.67	2.33±0.38	0.35±0.06	0.04±0.01
WW	2.48±0.43	8.88±1.51	2.38±0.41	0.49±0.09	0.09±0.02
WZ	0.7±0.11	2.26±0.33	0.56±0.08	0.1±0.02	0.02±0
ZZ	0.02±0	0.06±0.01	0.02±0	0±0	0±0
Z + jets	1.29±0.25	2.22±0.42	0.78±0.14	0.17±0.03	0.04±0.01
Non-W	27.8±8.33	26.6±7.97	9.07±2.72	2.22±1.78	0.32±0.5
Total background	196±31.7	311±51.1	111±14.7	39.6±4.89	9.37±1.25
WH115	0.16±0.02	0.65±0.08	0.16±0.02	0.03±0	0±0
Data	148	268	95	28	4

Table 3: Background summary table for 1-ST tag category.

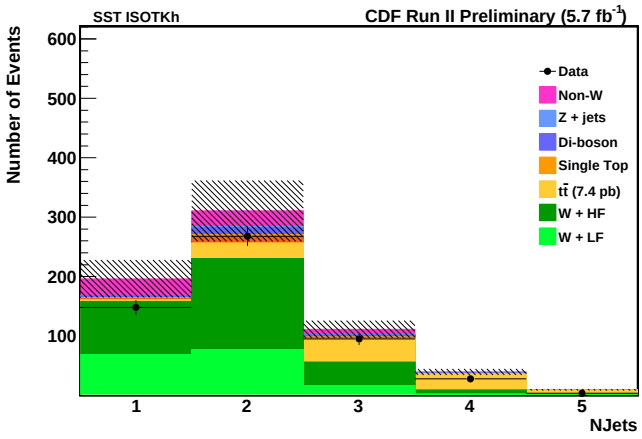

Figure 5: Number of expected and observed events for 1-ST tag category.

Sources	1jet	2jet	3jet	4jet	≥5jet
Pretag Events	32488	6544	1145	235	44
W + LF	0.13±0.05	0.46±0.17	0.22±0.09	0.05±0.02	0.01±0
W + bb	3.47±1.23	10.9±3.84	4.06±1.41	0.72±0.27	0.13±0.07
W + cc	0.15±0.05	0.76±0.25	0.47±0.16	0.12±0.04	0.04±0.02
W + cj	0.26±0.09	0.74±0.25	0.28±0.09	0.05±0.02	0.01±0.01
t#bart (7.4 pb)	0.32±0.07	7.85±1.8	15.7±3.54	16.2±3.61	4.88±1.08
Single Top S	0.15±0.03	2.1±0.49	0.6±0.14	0.16±0.04	0.04±0.01
Single Top T	0.09±0.02	0.66±0.16	0.6±0.14	0.14±0.03	0.03±0.01
WW	0±0	0.06±0.01	0.06±0.01	0.03±0.01	0±0
WZ	0.11±0.02	0.54±0.12	0.13±0.03	0.01±0	0.01±0
ZZ	0±0	0.01±0	0±0	0±0	0±0
Z + jets	0.01±0	0.08±0.02	0.05±0.01	0.01±0	0±0
Non-W	1.64±0.49	1.13±0.34	0.23±0.5	0.11±0.5	0.03±0.5
Total background	6.33±1.47	25.4±5.04	22.4±4.22	17.6±3.74	5.18±1.21
WH115	0.02±0.01	0.27±0.06	0.08±0.02	0.01±0	0±0
Data	4	21	19	18	5

Table 4: Background summary table for ST+ST tag category.

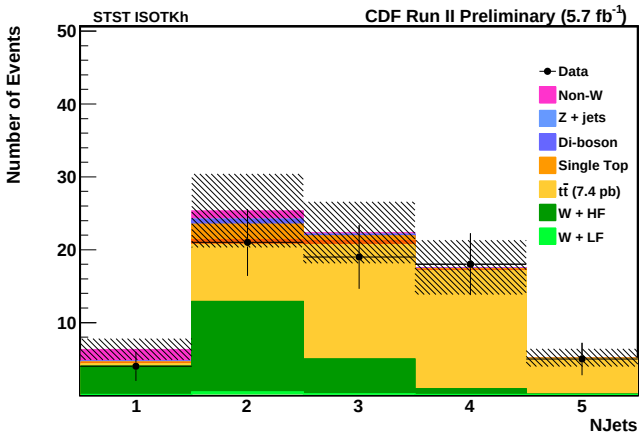

Figure 6: Number of expected and observed events for ST+ST tag category.

Sources	1jet	2jet	3jet	4jet	≥5jet
Pretag Events	32488	6544	1145	235	44
W + LF	0.16±0.05	1.12±0.43	0.45±0.2	0.1±0.08	0.02±0.01
W + bb	2.22±0.72	9.77±3.06	3.26±1.04	0.72±0.25	0.14±0.07
W + cc	0.31±0.1	2.02±0.66	1.15±0.38	0.31±0.11	0.06±0.03
W + cj	0.53±0.17	1.98±0.65	0.68±0.23	0.14±0.05	0.02±0.01
t#bart (7.4 pb)	0.24±0.05	5.96±0.93	13±2.14	13.6±2.29	4.47±0.81
Single Top S	0.08±0.02	1.51±0.24	0.48±0.08	0.12±0.02	0.02±0
Single Top T	0.07±0.01	0.55±0.1	0.43±0.07	0.11±0.02	0.02±0
WW	0.02±0	0.2±0.04	0.13±0.02	0.06±0.01	0.03±0.01
WZ	0.08±0.02	0.38±0.05	0.09±0.01	0.03±0.01	0±0
ZZ	0±0	0.01±0	0±0	0±0	0±0
Z + jets	0.02±0	0.09±0.02	0.06±0.01	0.02±0.01	0.01±0
Non-W	1.68±0.51	1.7±0.51	1.56±0.47	0.76±0.61	0.25±0.5
Total background	5.4±1.12	25.3±4.6	21.3±2.87	16±2.45	5.05±0.97
WH115	0.01±0	0.21±0.03	0.06±0.01	0.01±0	0±0
Data	6	19	15	12	4

Table 5: Background summary table for ST+JP tag category.

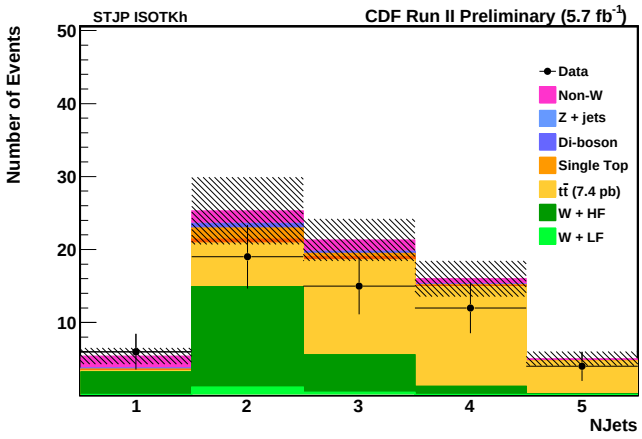

Figure 7: Number of expected and observed events for ST+JP tag category.

Sources	1jet	2jet	3jet	4jet	≥5jet
Pretag Events	32488	6544	1145	235	44
W + LF	0.67±0.23	3.1±0.91	1.39±0.46	0.26±0.1	0.04±0.03
W + bb	1.14±0.35	7.04±2.14	2.99±0.92	0.74±0.25	0.13±0.06
W + cc	0.22±0.07	1.97±0.62	1.25±0.4	0.35±0.12	0.08±0.04
W + cj	0.38±0.12	1.93±0.61	0.74±0.24	0.16±0.06	0.03±0.01
t#bart (7.4 pb)	0.13±0.02	3.85±0.5	9.73±1.32	10.1±1.4	3.54±0.52
Single Top S	0.05±0.01	0.92±0.12	0.35±0.05	0.09±0.01	0.02±0
Single Top T	0.05±0.01	0.49±0.07	0.38±0.06	0.08±0.01	0.02±0
WW	0.02±0	0.24±0.04	0.14±0.02	0.05±0.01	0.01±0
WZ	0.02±0	0.26±0.03	0.09±0.01	0.02±0	0±0
ZZ	0±0	0.01±0	0±0	0±0	0±0
Z + jets	0.02±0.01	0.12±0.03	0.07±0.02	0.03±0.01	0.01±0
Non-W	1.19±0.36	0.76±0.23	0.75±0.23	0.4±0.5	0.09±0.5
Total background	3.89±0.69	20.7±3.56	17.9±2.17	12.3±1.58	3.96±0.73
WH115	0.01±0	0.12±0.01	0.04±0	0.01±0	0±0
Data	3	15	16	17	4

Table 6: Background summary table for ST+RomaNN tag category.

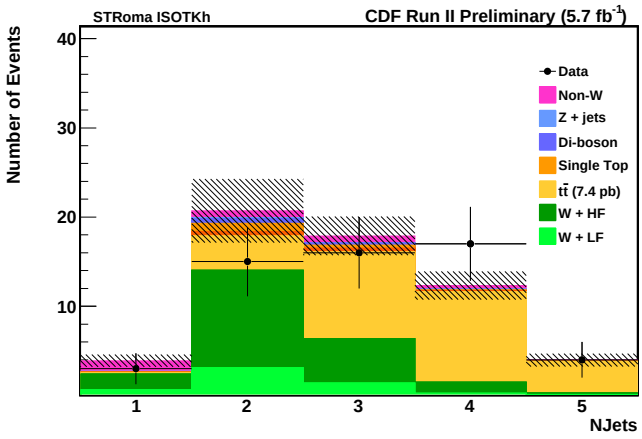

Figure 8: Number of expected and observed events for ST+RomaNN tag category.

$M(H)$	$\sigma(p\bar{p} \to W^{\pm}H)$	Br$(H \to b\bar{b})$
100	0.298 pb	0.812
105	0.253 pb	0.796
110	0.216 pb	0.770
115	0.186 pb	0.732
120	0.160 pb	0.679
125	0.138 pb	0.610
130	0.119 pb	0.527
135	0.104 pb	0.436
140	0.090 pb	0.344
145	0.079 pb	0.256
150	0.069 pb	0.176

Table 7: Theoretical cross section and branching ratio to $b\bar{b}$ for a variety of Higgs masses.

b-tagging category	IsoTrk Reco	Trigger	ISR/FSR/PDF	JES	b-tagging	Total
One tag	8.85%	2%	8.4%	4.7%	4.3%	13.9%
ST + ST	8.85%	2%	7.1%	1.7%	8.6%	14.5%
ST + JP	8.85%	2%	6.4%	2.4%	8.1%	14.0%
ST + RomaNN	8.85%	2%	19.5%	1.9%	13.6%	25.5%

Table 8: Systematic uncertainties for IsoTrks.

4 Signal Acceptance

Samples of PYTHIA $WH \to l\nu b\bar{b}$ Monte Carlo with Higgs boson masses between 100 GeV and 150 GeV are used to estimate $\epsilon^{MC}_{WH\to l\nu b\bar{b}}$. The MC samples were generated with beam conditions which approximate real data periods, for run periods 0-18.

Table 7 shows the NNLO WH production cross section and the branching ratio of $H \to b\bar{b}$. The cross sections and the branching ratios in table 7 are multiplied with the integrated luminosity, 5.6 fb^{-1}, and the overall event detection efficiencies to produce the number of expected WH events as shown in Table 3 - 6.

4.1 Other Systematic Uncertainties on Acceptance

The systematic uncertainties on the acceptance include uncertainties from the jet energy scale, initial and final state radiation contribution, and the b-tagging scale factor, which are very similar to the uncertainty estimates as described in the standard isolated track analysis [1]. Total systematic uncertainties are listed in Table 8.

5 Kinematic Distributions

The kinematic distribution for all discriminant input variables and NN output distributions have been thoroughly examined to establish proper modeling using pretag sample, see Figures 9 - 13. The data and MC background estimates are in good agreement. The same NN inputs and output distributions after b-tagging can be found in Appendix:

- Figure 19 - 23 for STST tags;
- Figure 24 - 28 for STJP tags;
- Figure 29 - 33 for STRoma tags;
- Figure 34 - 38 for SST tags.

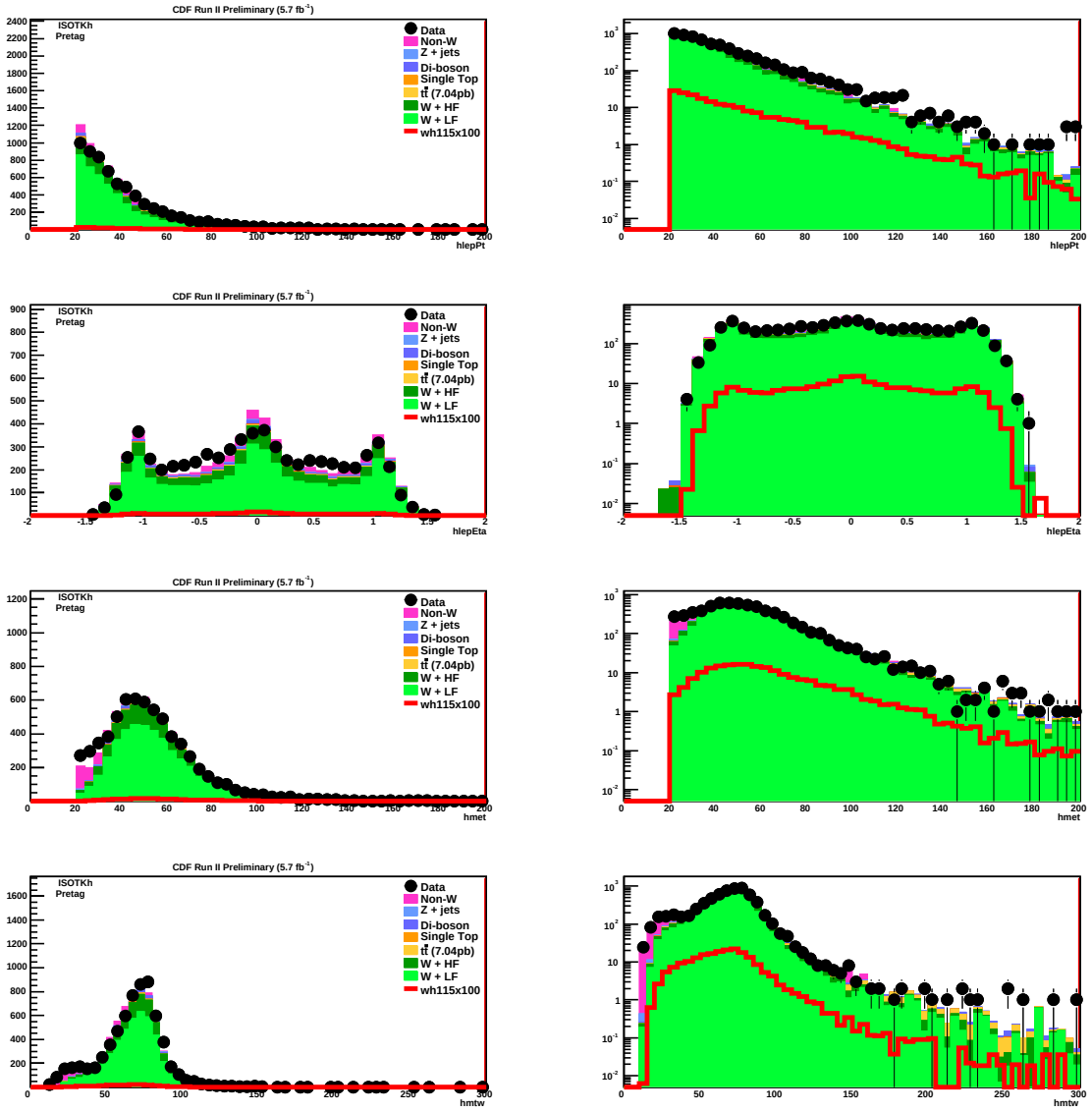

Figure 9: Pretag kinematic distributions for isolated track p_T, η,$\not\!\!E_T$, and W transverse mass.

6 Shape Systematics

Since the entire histogroms of the BNN output in the selected signal region are used to extract the final result, the shape uncertainties affect the final sensitivity of this analysis.

We estimate Jet Energy Scale (JES) shape uncertainty by shifting the JES with $\pm$ 1 sigma from the nominal value. Figure 14-16 shows the comparison between nominal and $\pm$ 1 sigma shifted BNN templates for the signal and some main backgrounds, such

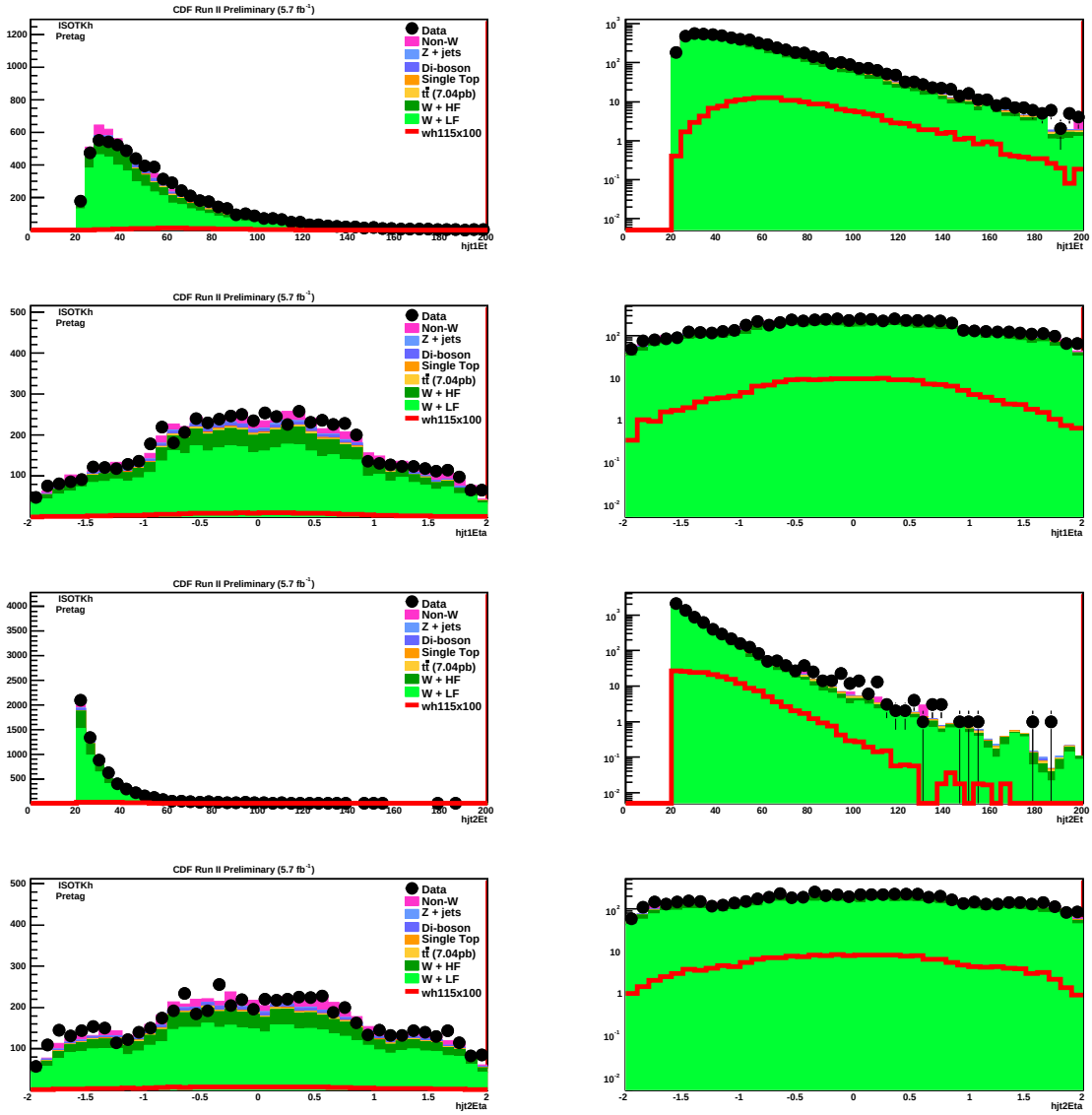

Figure 10: Pretag kinematic distributions for first jet E_T, η and second jet E_T, η.

as $W + b\bar{b}$ and $t\bar{t}$, respectively. To extract the limit, we do include the JES shape uncertainty for the signal and all the backgrounds (W+jets ($W + b\bar{b}$, $W + c\bar{c}$, Mistag), $t\bar{t}$, single top (s-channel, t-channel), dibosons (WW, WZ, ZZ), and Z+jets).

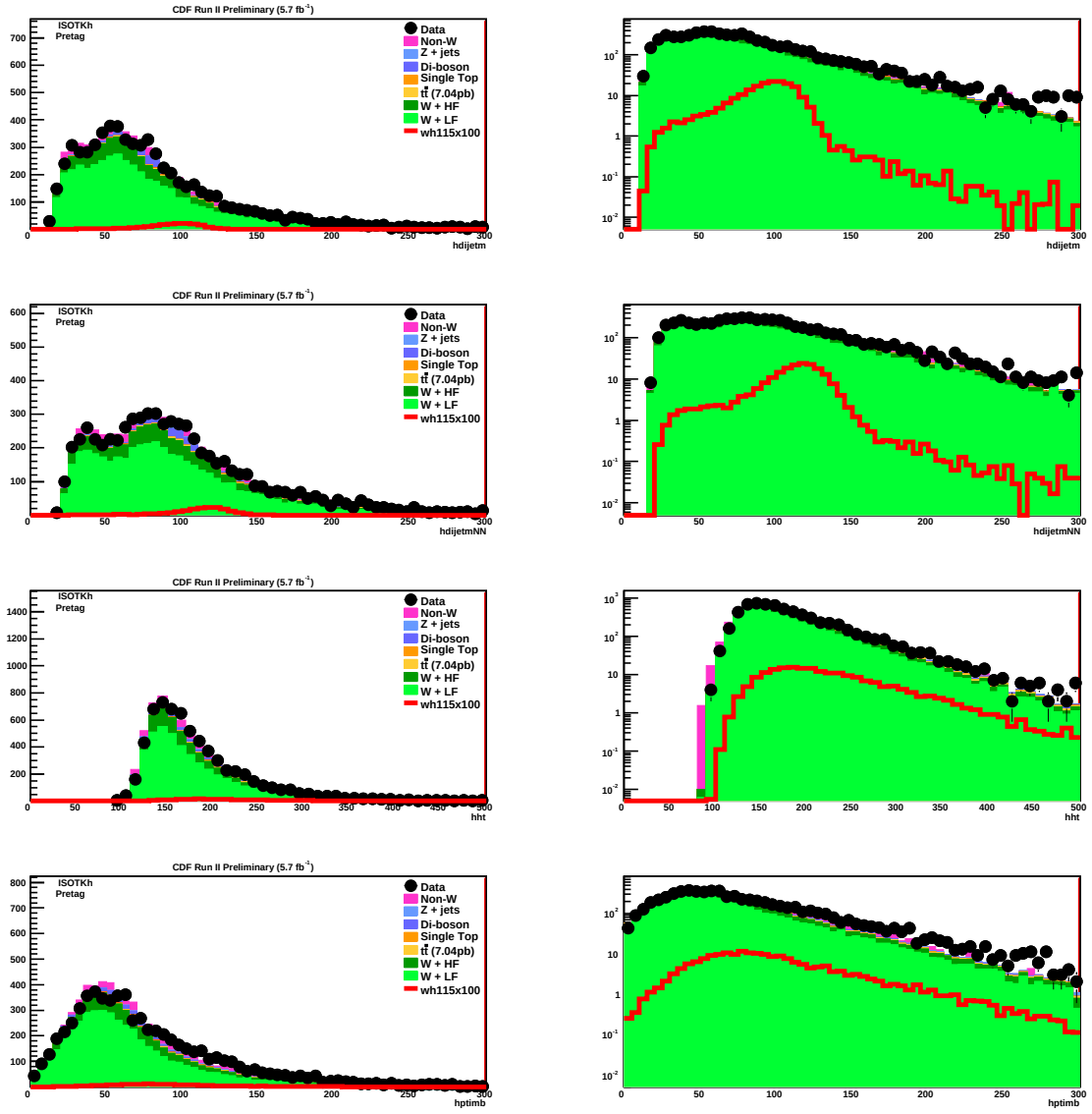

Figure 11: Pretag kinematic distributions for dijet mass before and after bjet energy correction, H_T, and P_T imbalance.

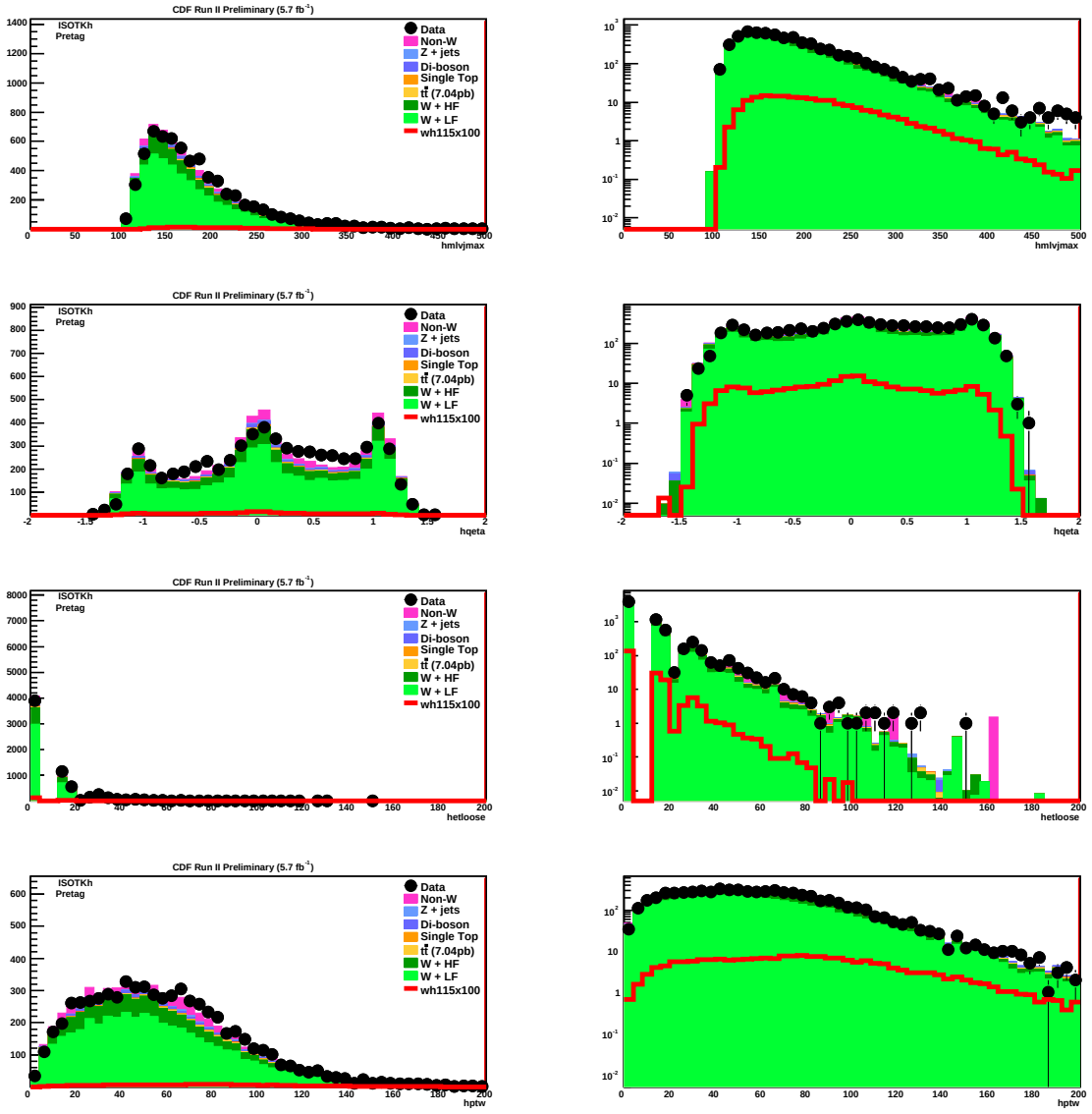

Figure 12: Pretag kinematic distributions for maximum of lvj mass, $\eta \times Q$, sum loose jet E_T, and P_T of W candidate.

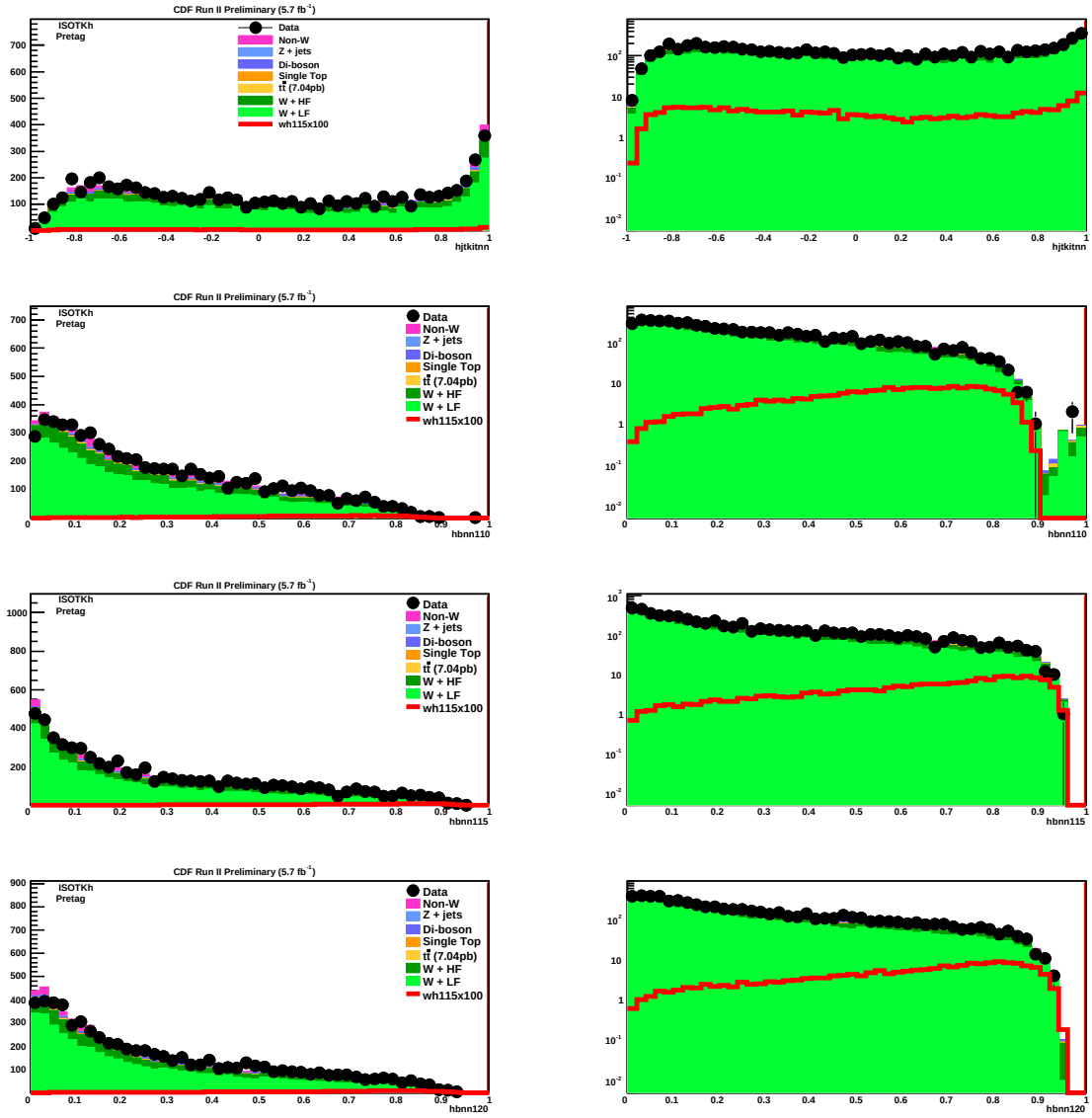

Figure 13: Pretag kinematic distributions for kitnn and Bnn output corresponds to m_H =110, 115, 120 GeV/c^2 respectively.

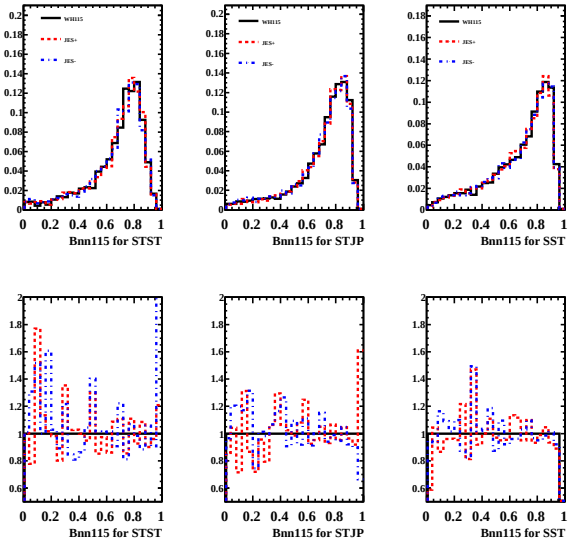

Figure 14: BNN output shape for default and ±1 sigma JES for WH signal (m_H = 115 GeV/c^2). From left to right, tight double(ST+ST), loose double(ST+JP and ST+RomaNN), and single tag(SST), respectively.

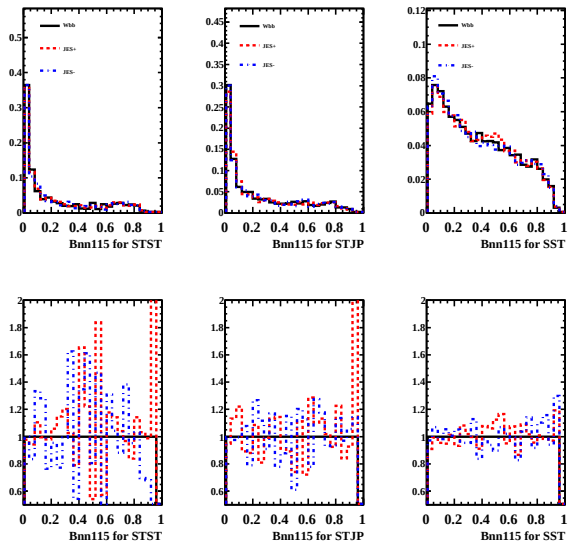

Figure 15: BNN output shape for default and ±1 sigma JES for $Wb\bar{b}$ (m_H = 115 GeV/c^2). From left to right, tight double(ST+ST), loose double(ST+JP and ST+RomaNN), and single tag(SST), respectively.

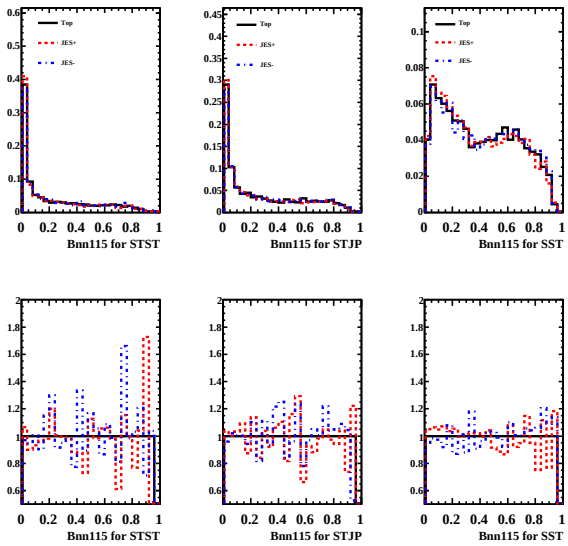

Figure 16: BNN output shape for default and ±1 sigma JES for $t\bar{t}$ ($m_H = 115$ GeV/c^2). From left to right, tight double(ST+ST), loose double(ST+JP and ST+RomaNN), and single tag(SST), respectively.

7 Results

Since there is no significant excess of events in the data compared to the background expectation, we fit the NN output distributions shown in Figure 17 and extract 95% C.L. upper limits for the four tag categories (1-ST, ST+ST, ST+JP and ST+RomaNN) using pseudo-experiments based on the background expectations.

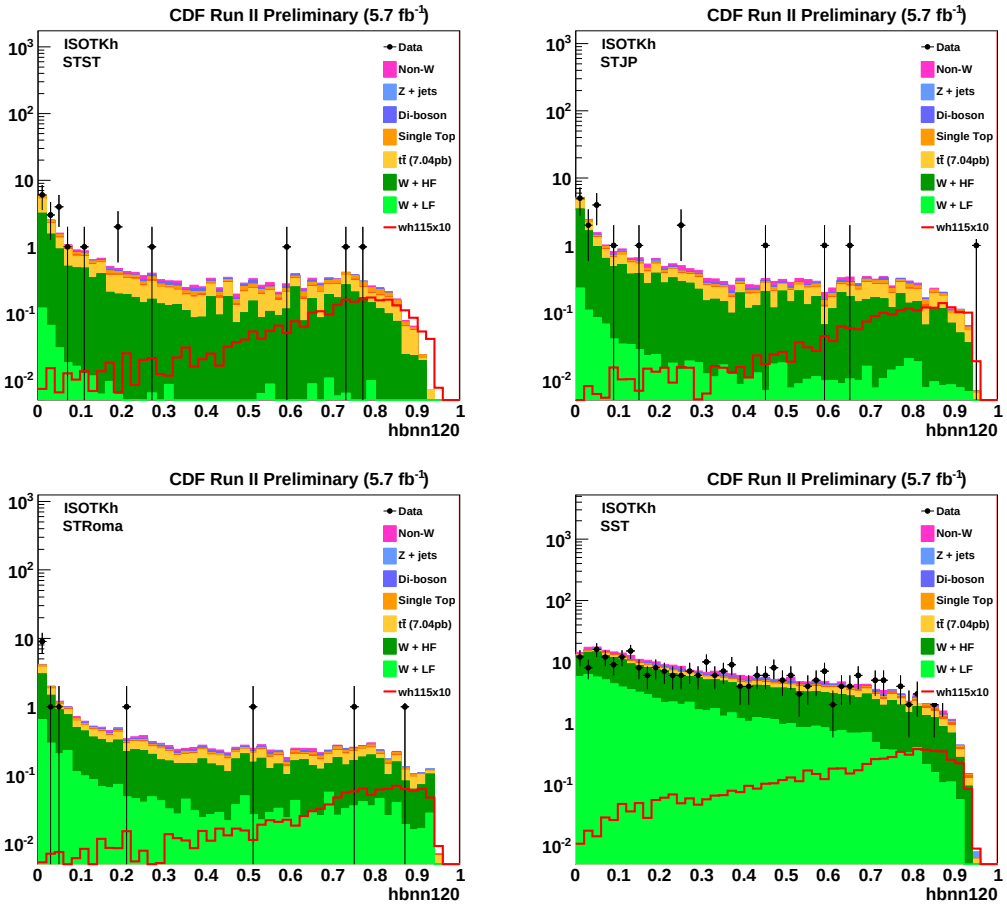

Figure 17: BNN data output in four b-tagging categories (STST, STJP, STRoma, SST) along with background expectations for the Higgs mass hypothesis at $m_H = 120$ GeV/c^2.

The following systematic uncertainties, up to the pretag acceptance, are treated as 100% correlated:

1. luminosity uncertainty
2. uncertainty on the SECVTX b-tag scale factor
3. Jet probability scale factor

CDF Run II Preliminary 5.7 fb^{-1} Limits for Combined Lepton and Tag Categories		
M(H)	Observed Limit	Expected Limit
100	5.4	10.7
105	6.4	12.0
110	7.5	13.8
115	9.9	14.9
120	13.8	18.5
125	18.1	21.2
130	25.4	28.5
135	34.2	37.6
140	57.4	54.0
145	76.5	74.1
150	135.0	131.2

Table 9: Expected and observed limits as a function of Higgs mass for combining the combined all b-tag categories.

4. RomaNN scale factor.

Table 9 details the expected and observed limits at the various Higgs mass points for the combined search across lepton types and tag categories. Figure 18 shows the observed limits and the expected limits with 1σ and 2σ pseudo experiment bands.

8 Conclusions

We present a new selection of W events to be used in the $WH \to l\nu b\bar{b}$ analysis. The new events are selected by requiring an isolated track with significant deposits of energy in the calorimeter that are primary from the decay of $W \to e\nu$ or $\tau\nu$ where the electron failed the standard electron selection or the τ decays into a single charged hadron (one-prong). We find that for the dataset corresponding to integrated luminosity of 5.7 fb^{-1}, the data agree with the SM background predictions within the systematic uncertainties. We therefore set upper limits on the Higgs production cross section times the $b\bar{b}$ branching ratio. We find $\sigma(p\bar{p} \to W^{\pm}H) \times \mathrm{Br}(H \to b\bar{b})$ with an observed limit 9.9 $\times$ SM (14.9 $\times$ SM expected) for $m_h = 115$ GeV/c^2 at 95% confidence level.

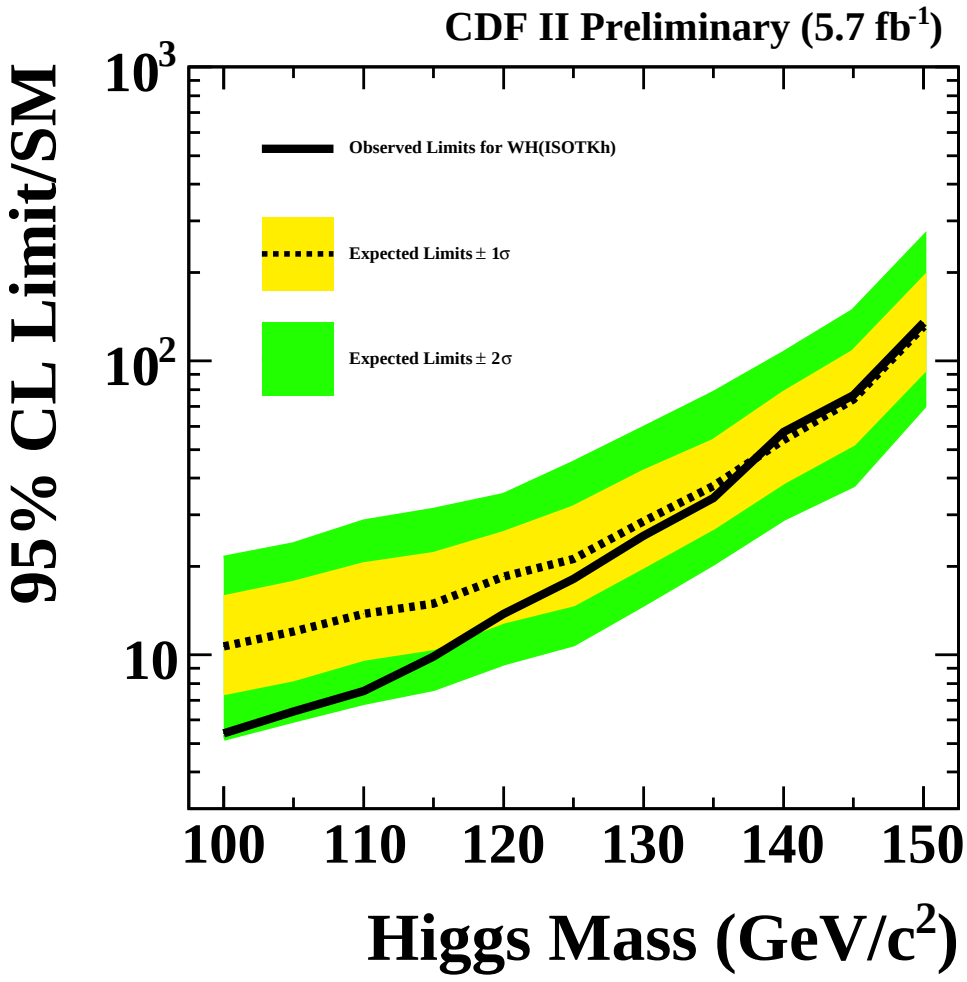

Figure 18: Expected and observed limts for combining all b-tag categories.

References

[1] Y. Nagai *et al.*, "Search for Higgs Boson Production in Association with a W Boson using $\int \mathcal{L}dt = 4.8$ fb^{-1}," CDF Note 10145.

[2] A. Buzatu, N. Krumnack, and A. Warburton, "Trigger Turnon Parametrizations for WH Search," CDF Note 9623.

[3] T. Chwalek *et al.*, "Update of the neural network b tagger for single-top analysis," CDF Note 8903.

[4] T. Aaltonen *et al.*, "Neural Network b-jet energy correction for WHNN analysis", CDF Note 9858.

[5] http://www.cs.toronto.edu/%7Eradford/fbm.software.html

[6] J. Adelman, T. Schwarz, J. Slaunwhite, et al. "Method II For You", CDF Note 9185

[7] http://www-cdf.fnal.gov/internal/physics/top/RunIIBtag/bTag.html

[8] http://www-cdf.fnal.gov/internal/physics/joint_physics/index.html

A Kinematic Distribution after Tagging

A.1 Kinematic Distributions after STST

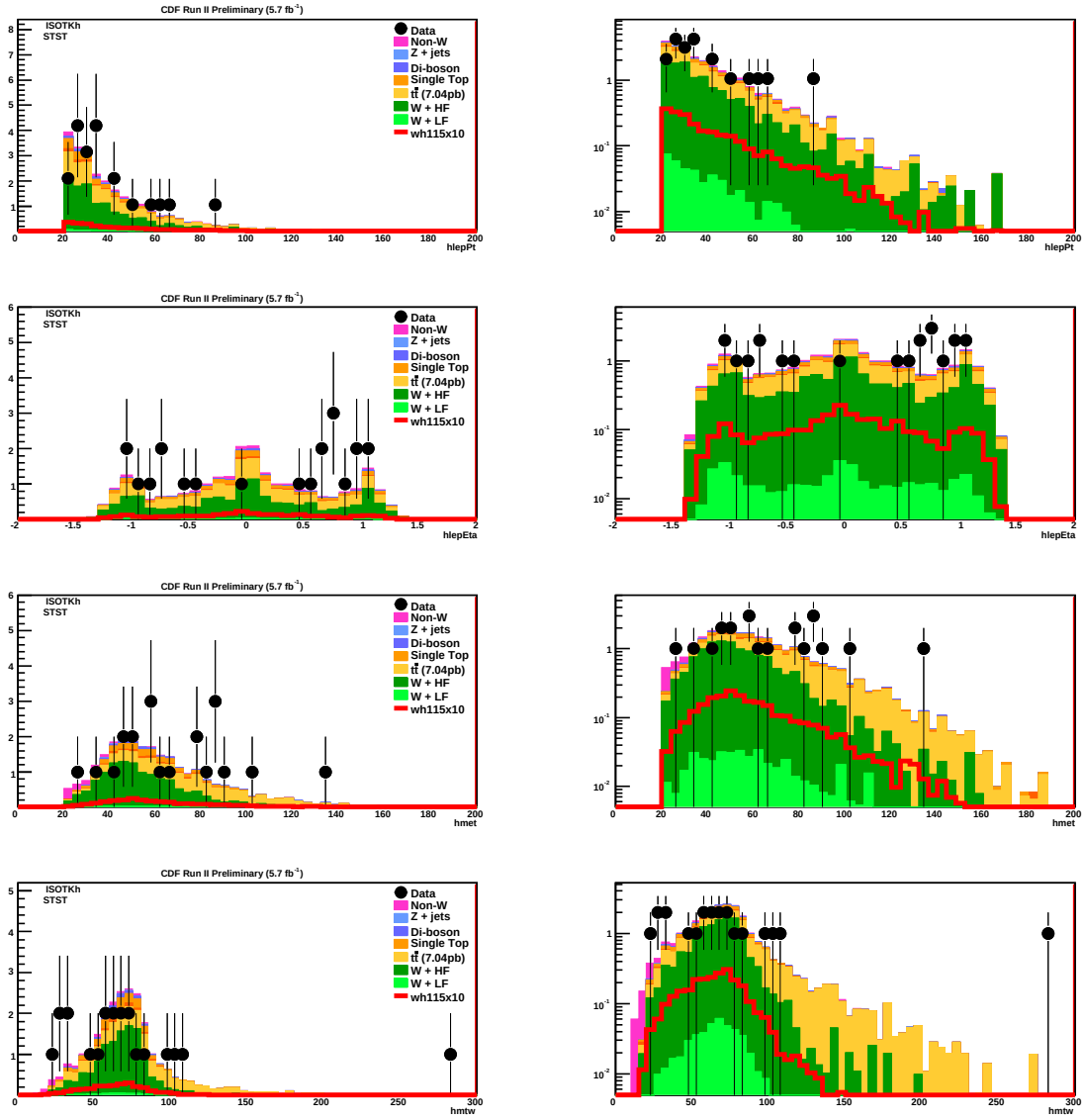

Figure 19: STST kinematic distributions for isolated track p_T, η,$\not\!\!E_T$, and W transverse mass.

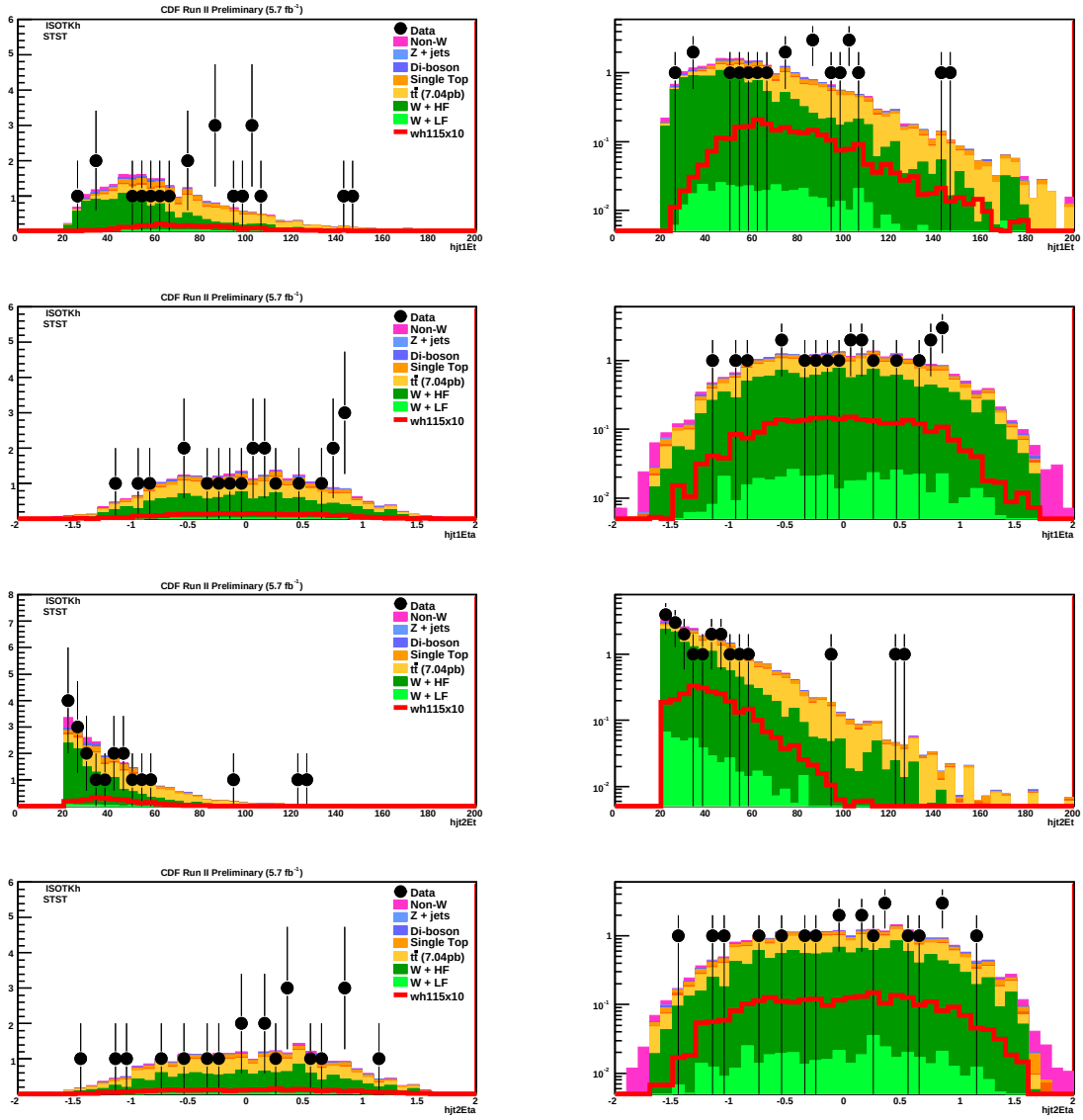

Figure 20: STST kinematic distributions for first jet E_T, η and second jet E_T, η.

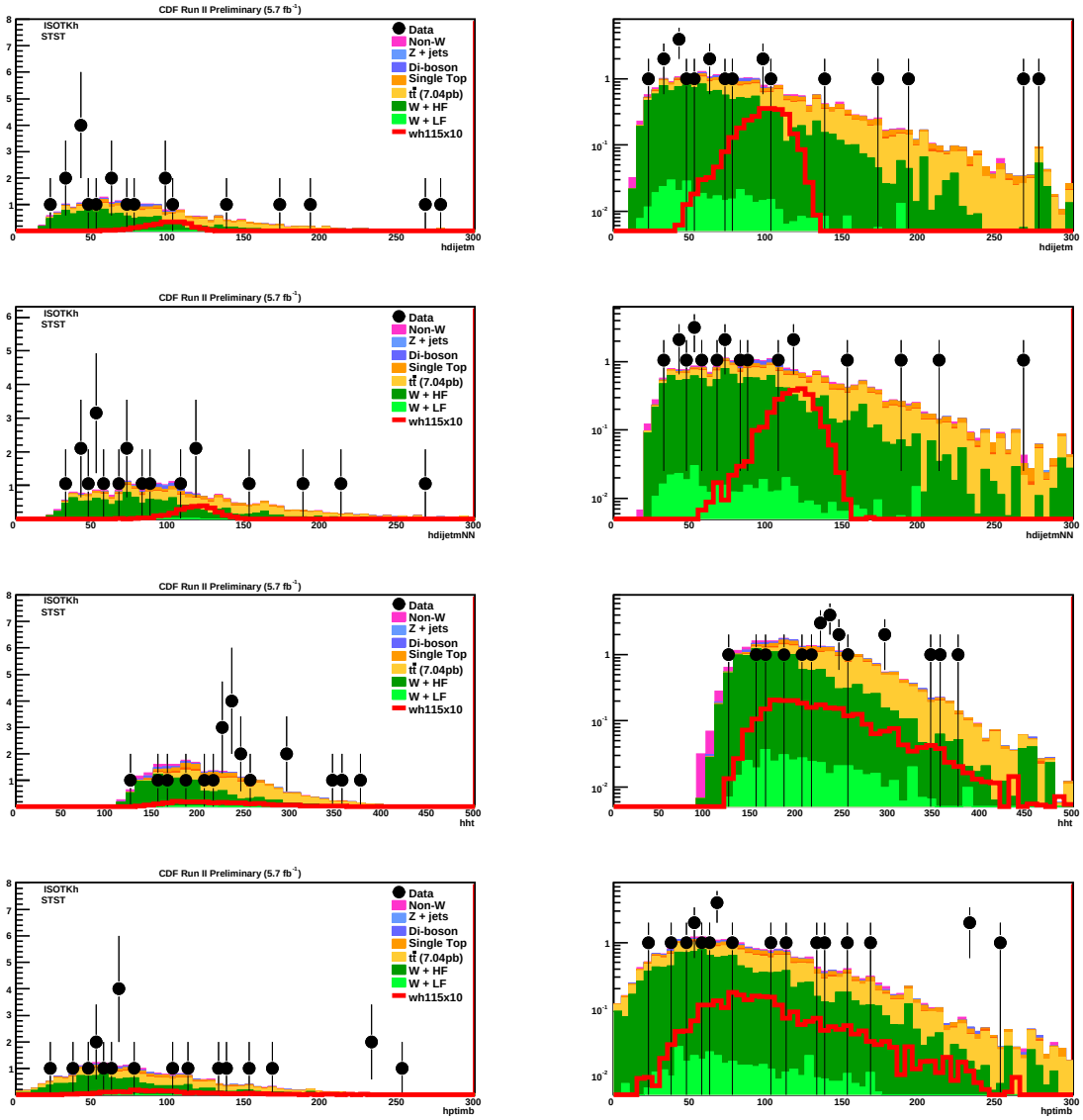

Figure 21: STST kinematic distributions for dijet mass before and after bjet energy correction, H_T, and P_T imbalance.

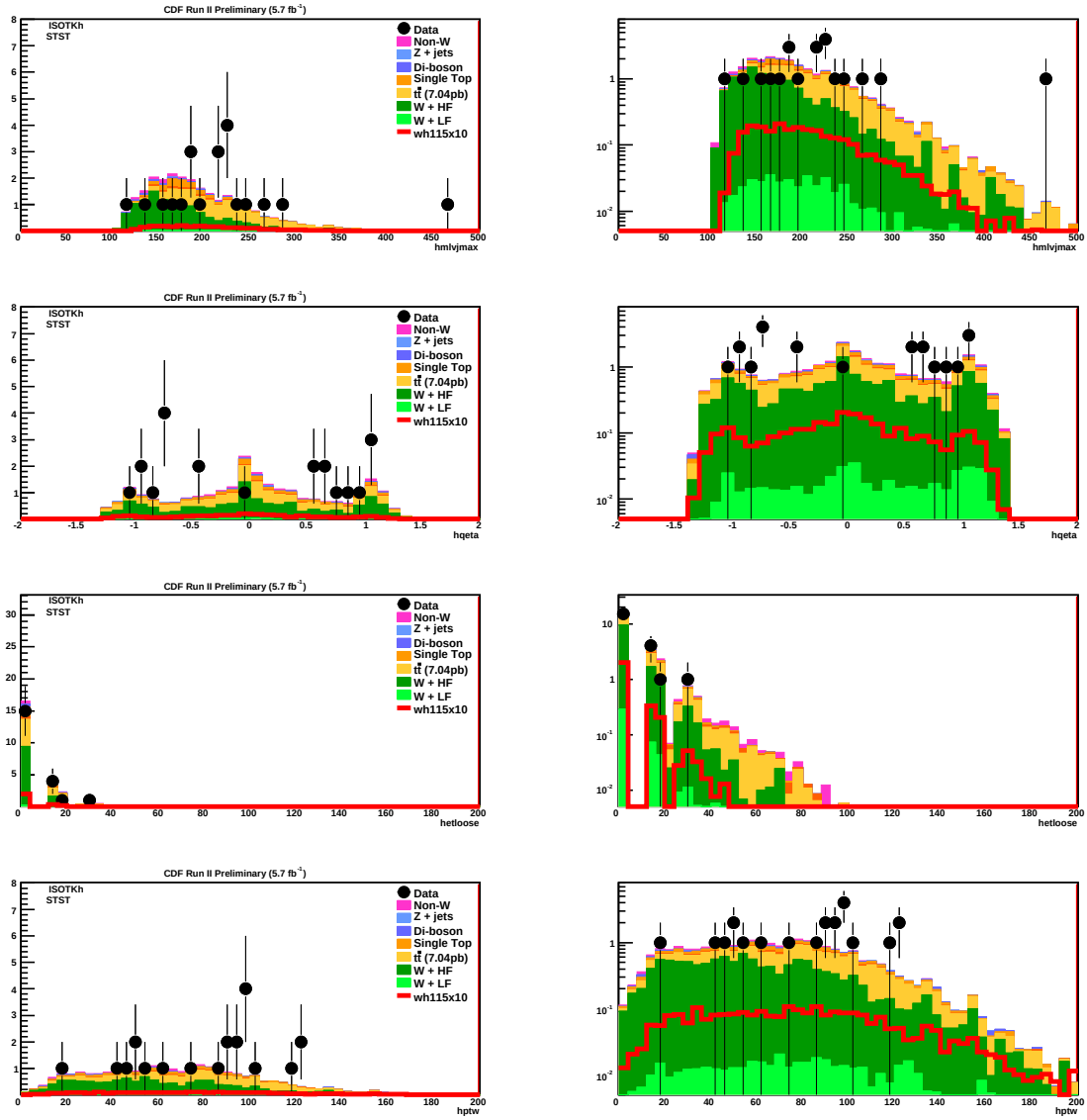

Figure 22: STST kinematic distributions for maximum of lvj mass, $\eta \times Q$, sum loose jet E_T, and P_T of W candidate.

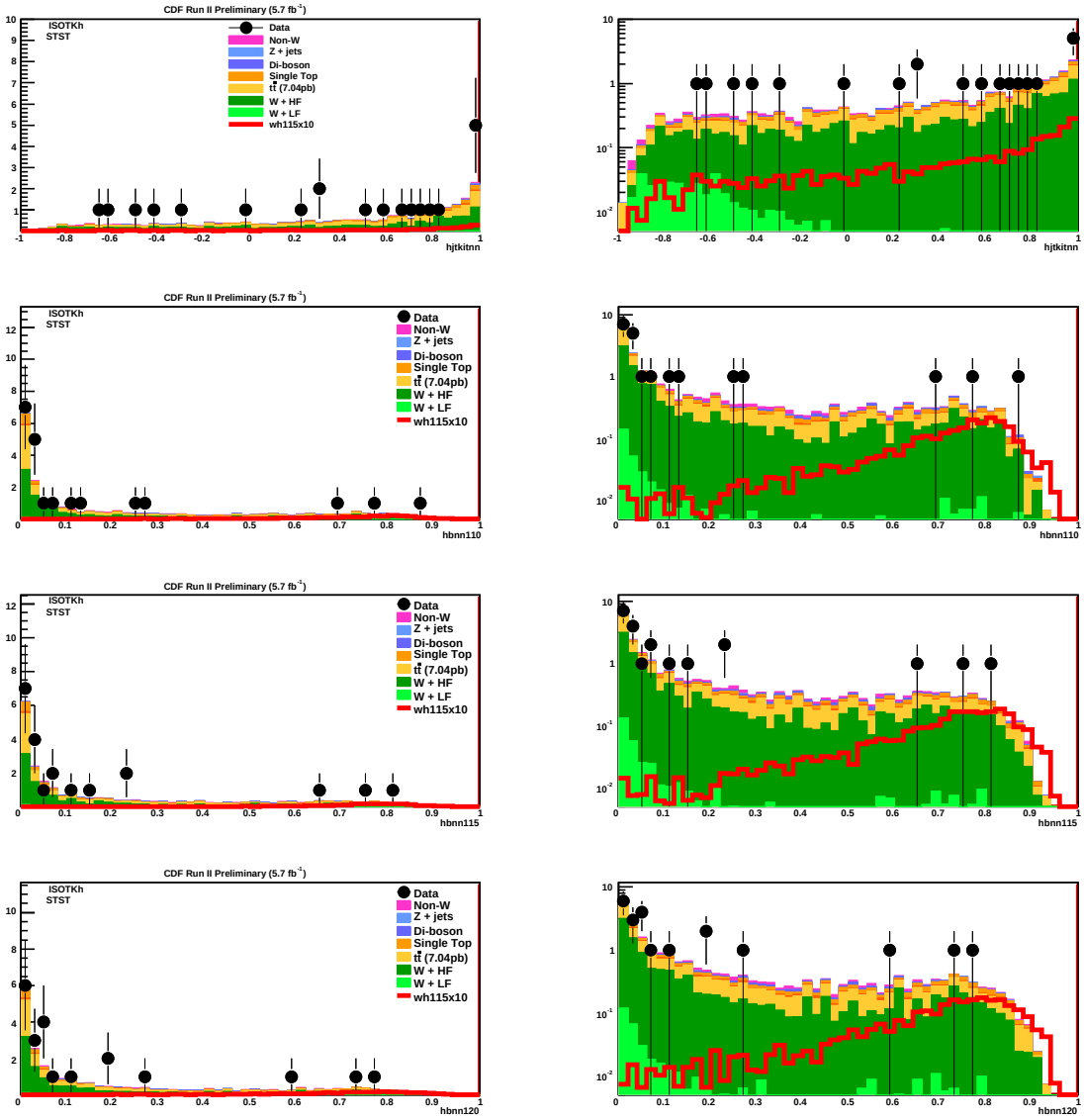

Figure 23: STST kinematic distributions for kitnn and Bnn output corresponds to m_H =110, 115, 120 GeV/c^2 respectively.

A.2 Kinematic Distributions after STJP

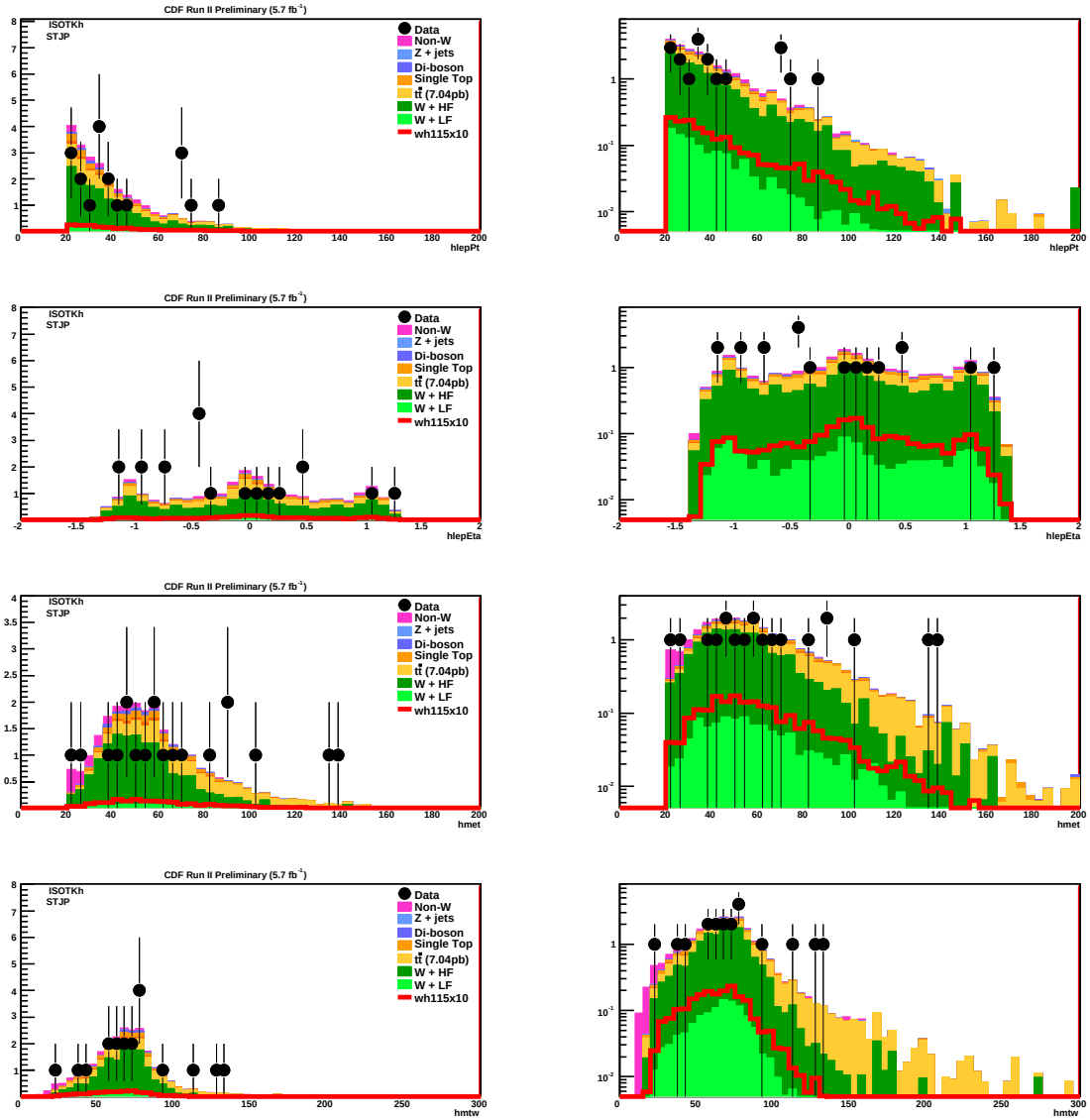

Figure 24: STJP kinematic distributions for isolated track p_T, η,$\not\!\!E_T$, and W transverse mass.

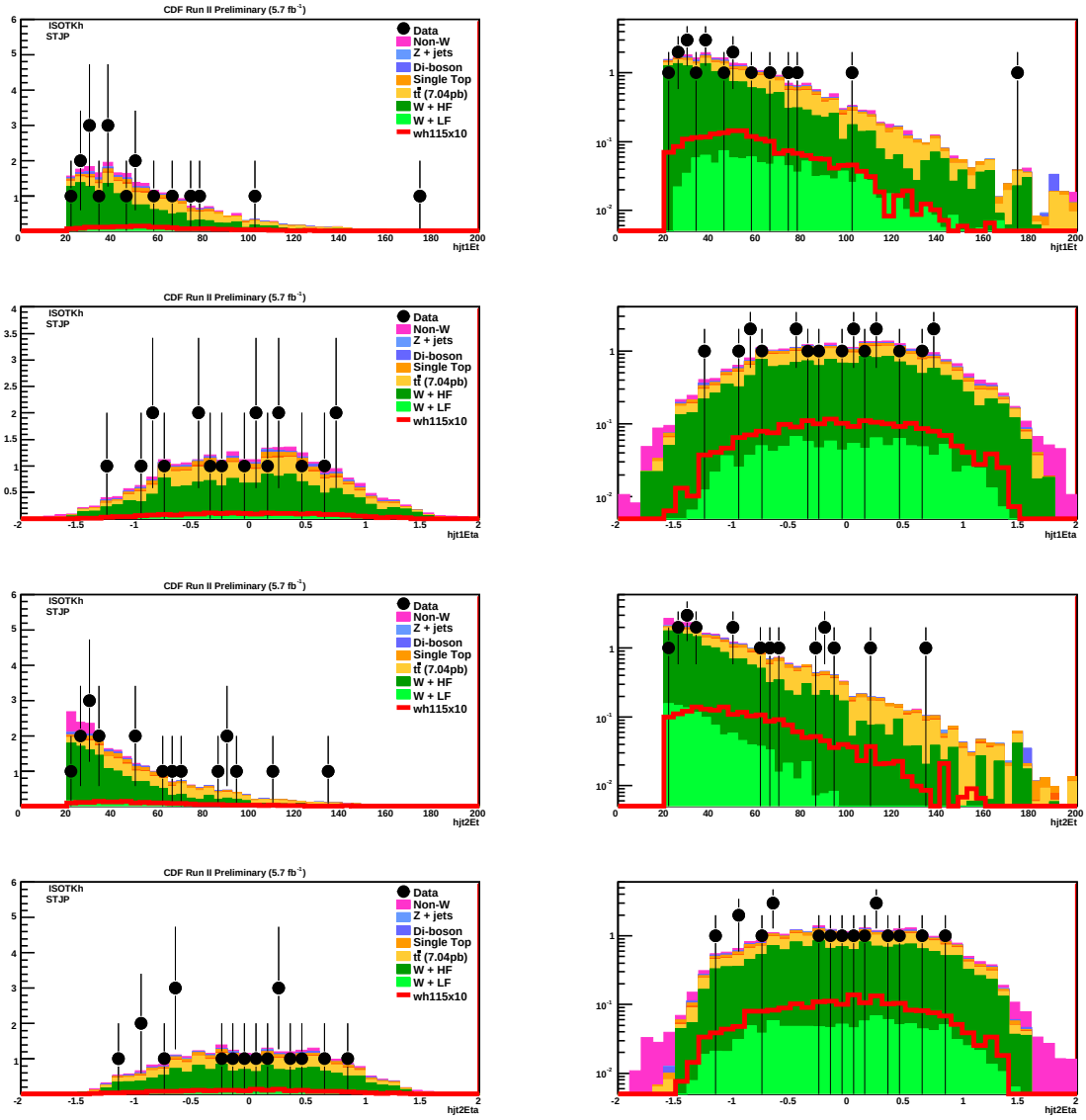

Figure 25: STJP kinematic distributions for first jet E_T, η and second jet E_T, η.

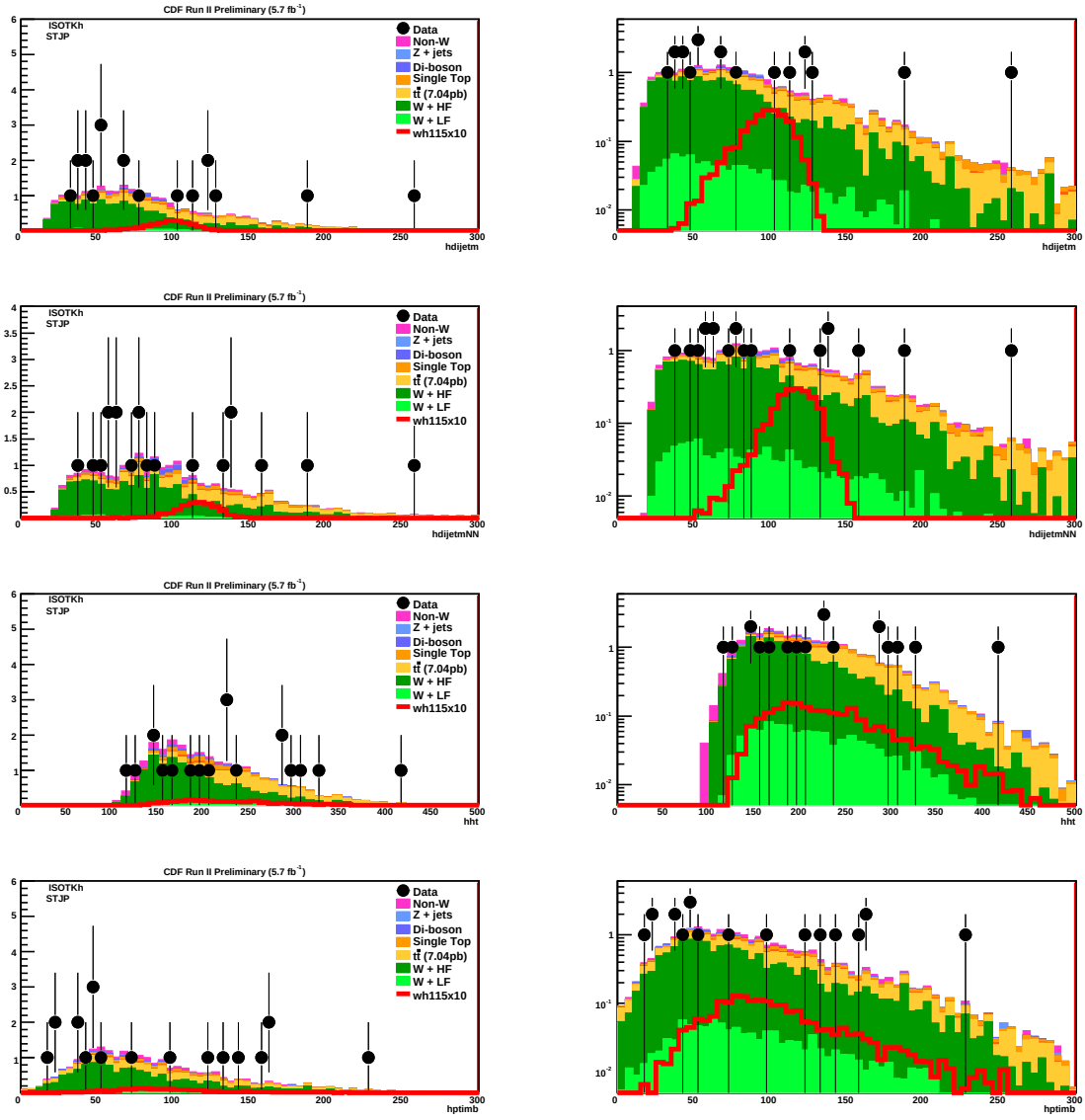

Figure 26: STJP kinematic distributions for dijet mass before and after bjet energy correction, H_T, and P_T imbalance.

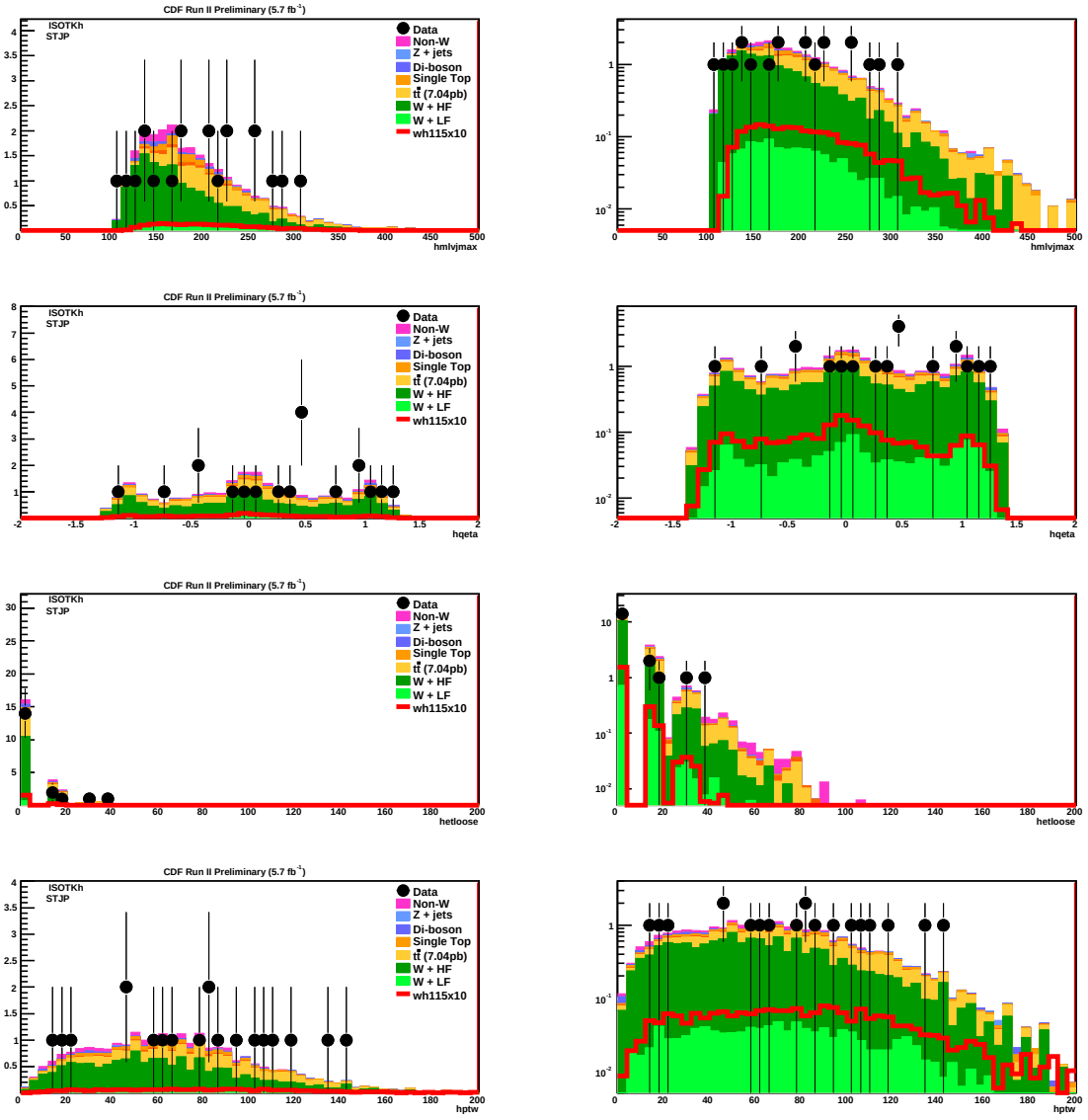

Figure 27: STJP kinematic distributions for maximum of lvj mass, $\eta \times Q$, sum loose jet E_T, and P_T of W candidate.

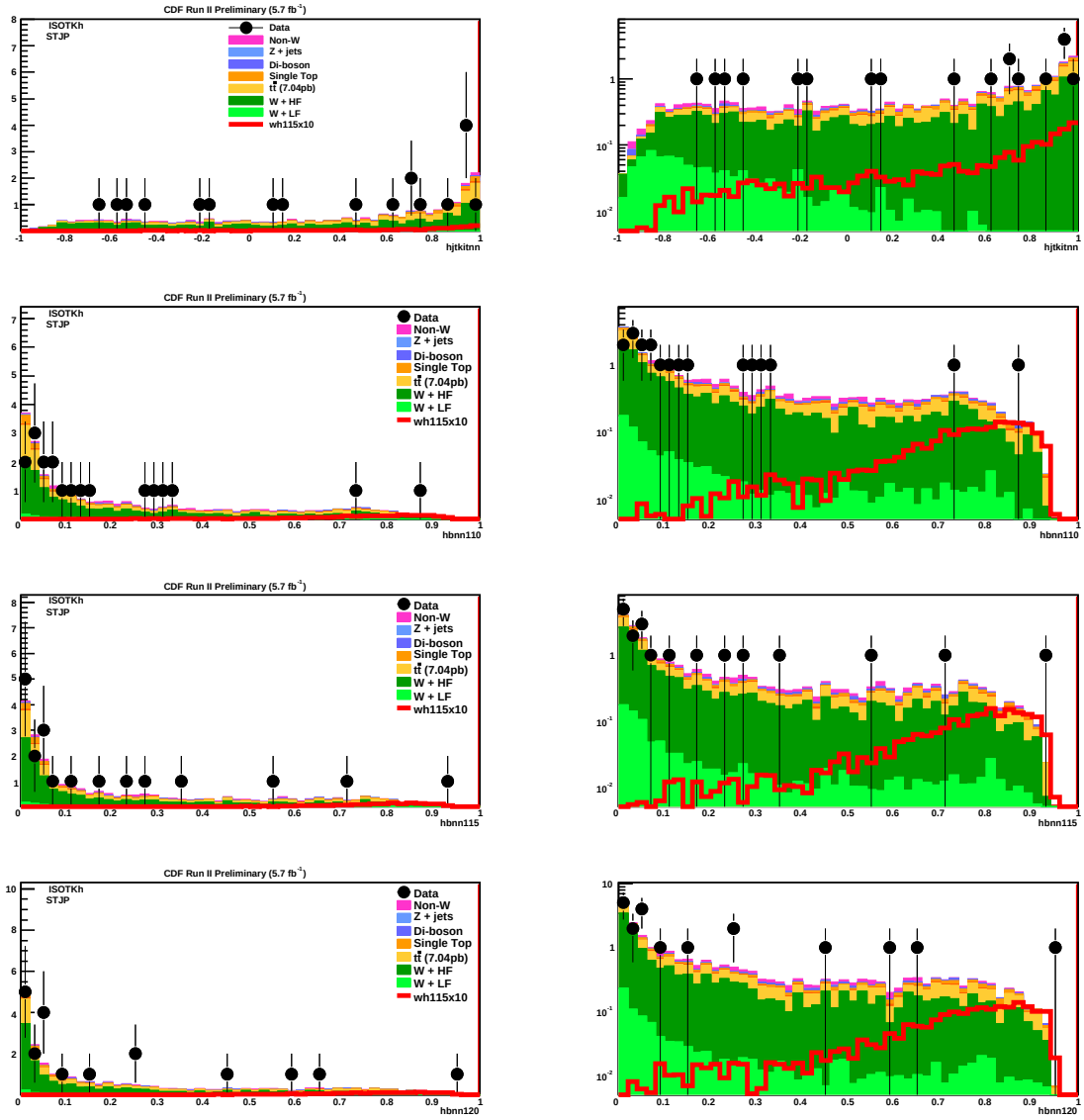

Figure 28: STJP kinematic distributions for kitnn and Bnn output corresponds to m_H =110, 115, 120 GeV/c^2 respectively.

A.3 Kinematic Distributions after STRoma

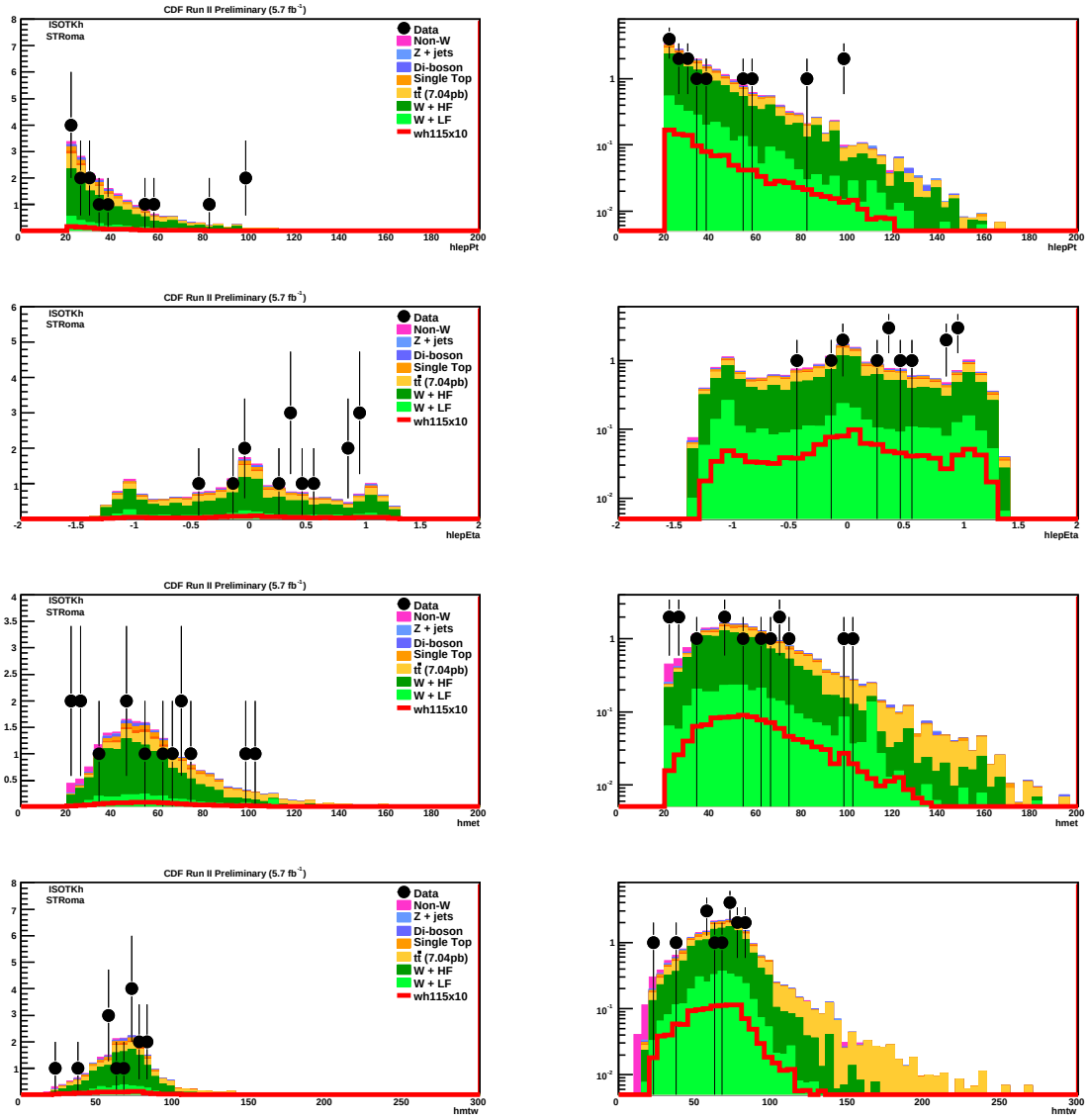

Figure 29: STRoma kinematic distributions for isolated track p_T, η,$\not\!\!E_T$, and W transverse mass.

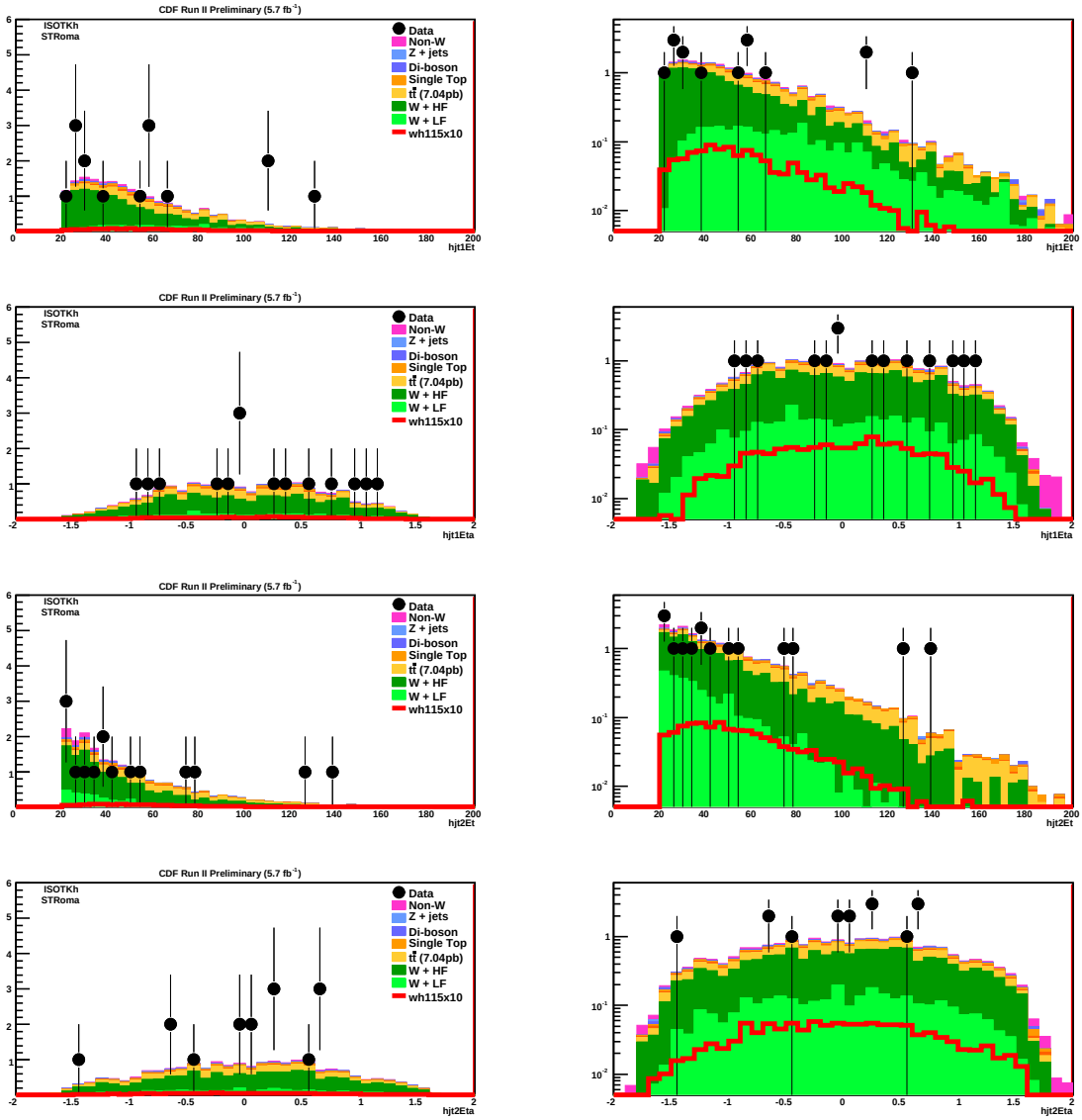

Figure 30: STRoma kinematic distributions for first jet E_T, η and second jet E_T, η.

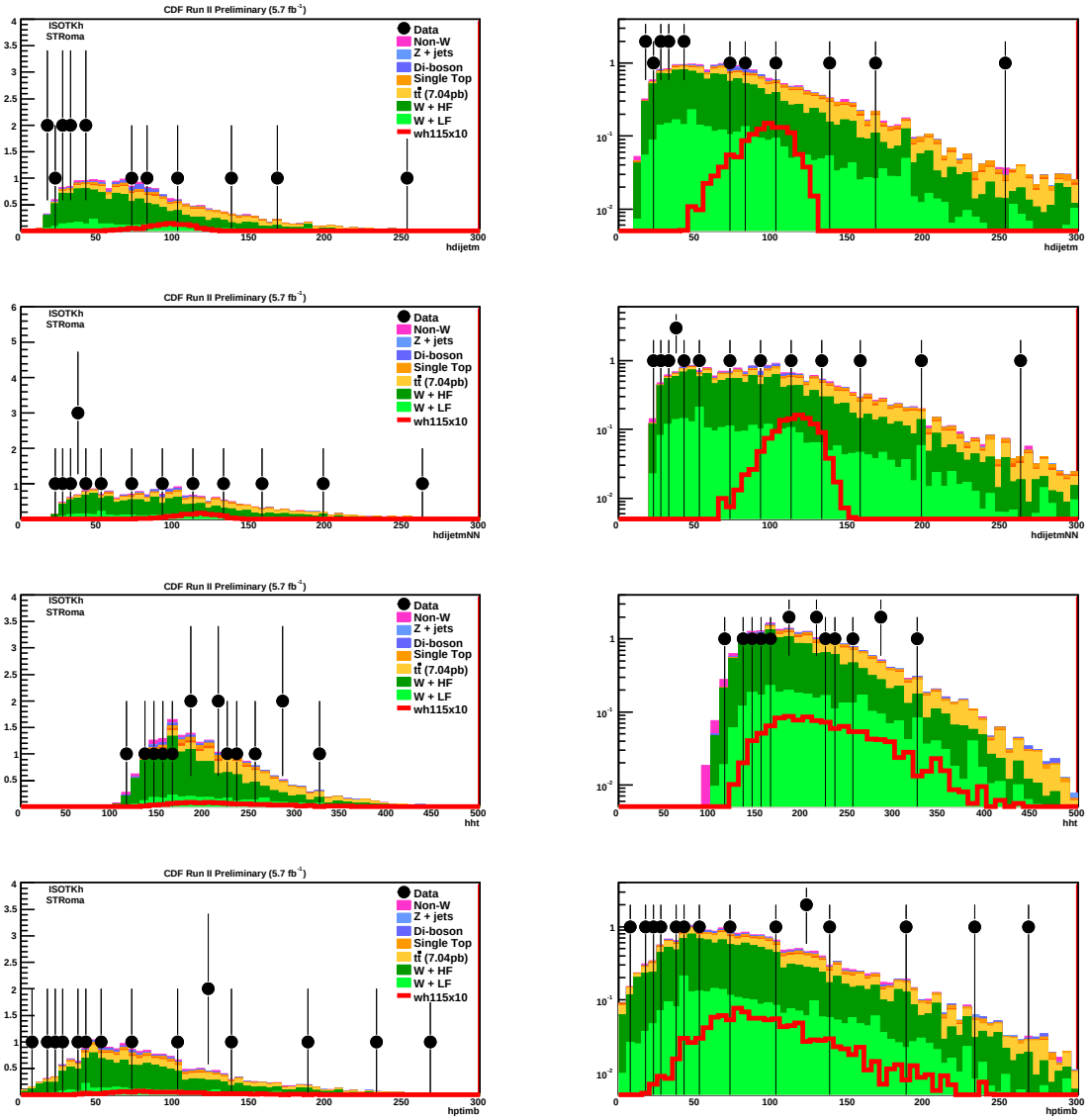

Figure 31: STRoma kinematic distributions for dijet mass before and after bjet energy correction, H_T, and P_T imbalance.

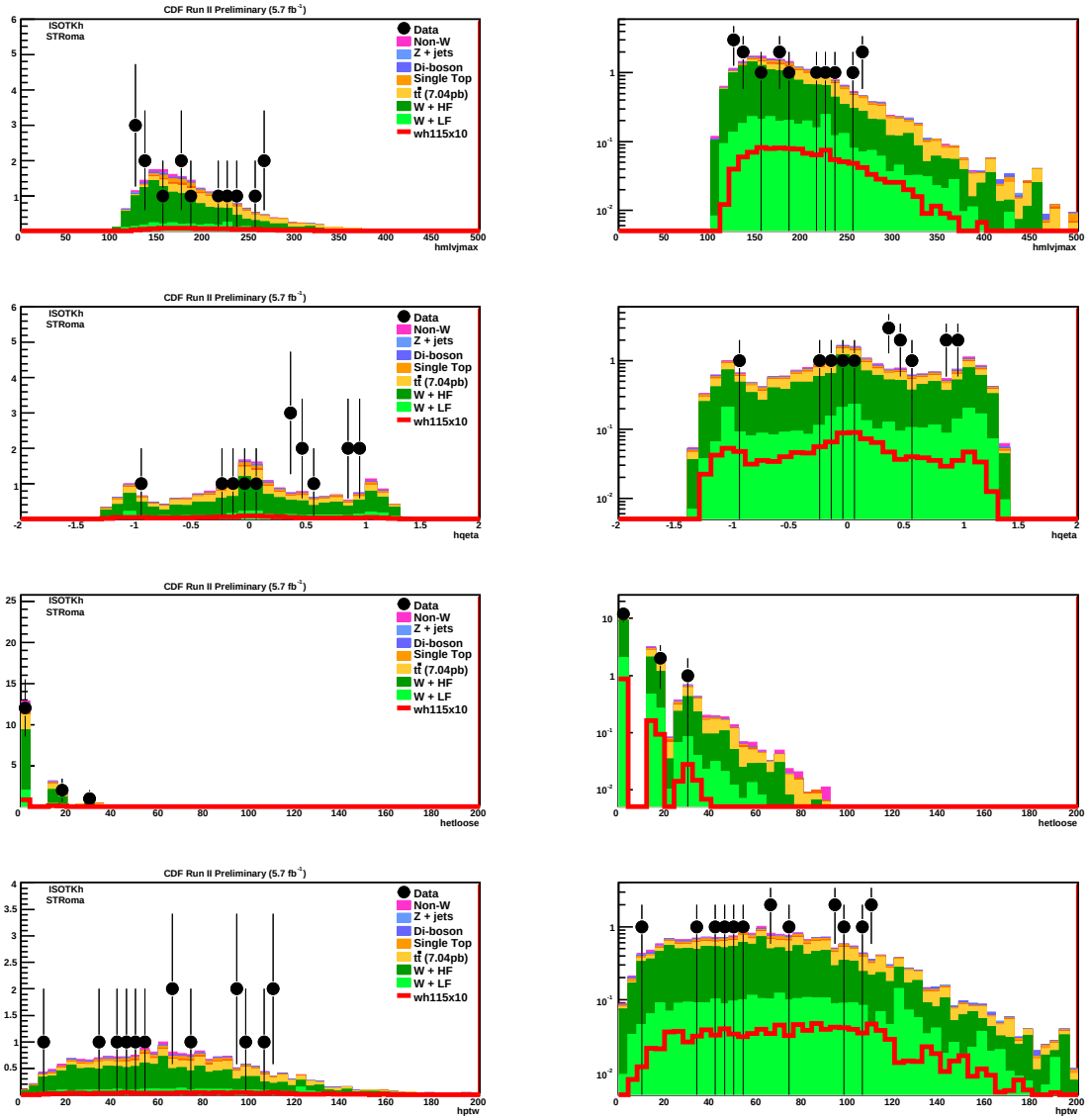

Figure 32: STRoma kinematic distributions for maximum of lvj mass, $\eta \times Q$, sum loose jet E_T, and P_T of W candidate.

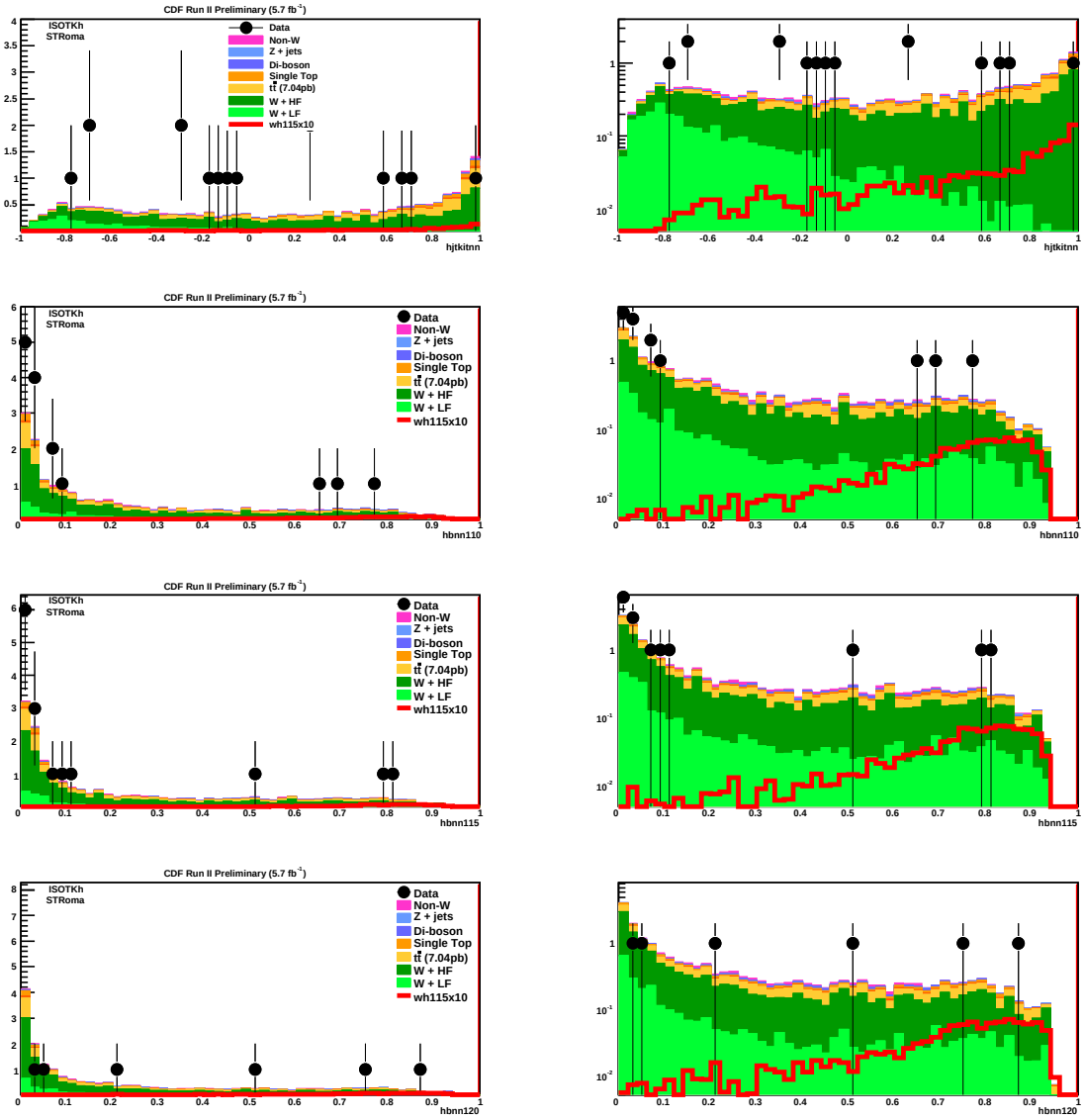

Figure 33: STRoma kinematic distributions for kitnn and Bnn output corresponds to m_H =110, 115, 120 GeV/c^2 respectively.

A.4 Kinematic Distributions after SST

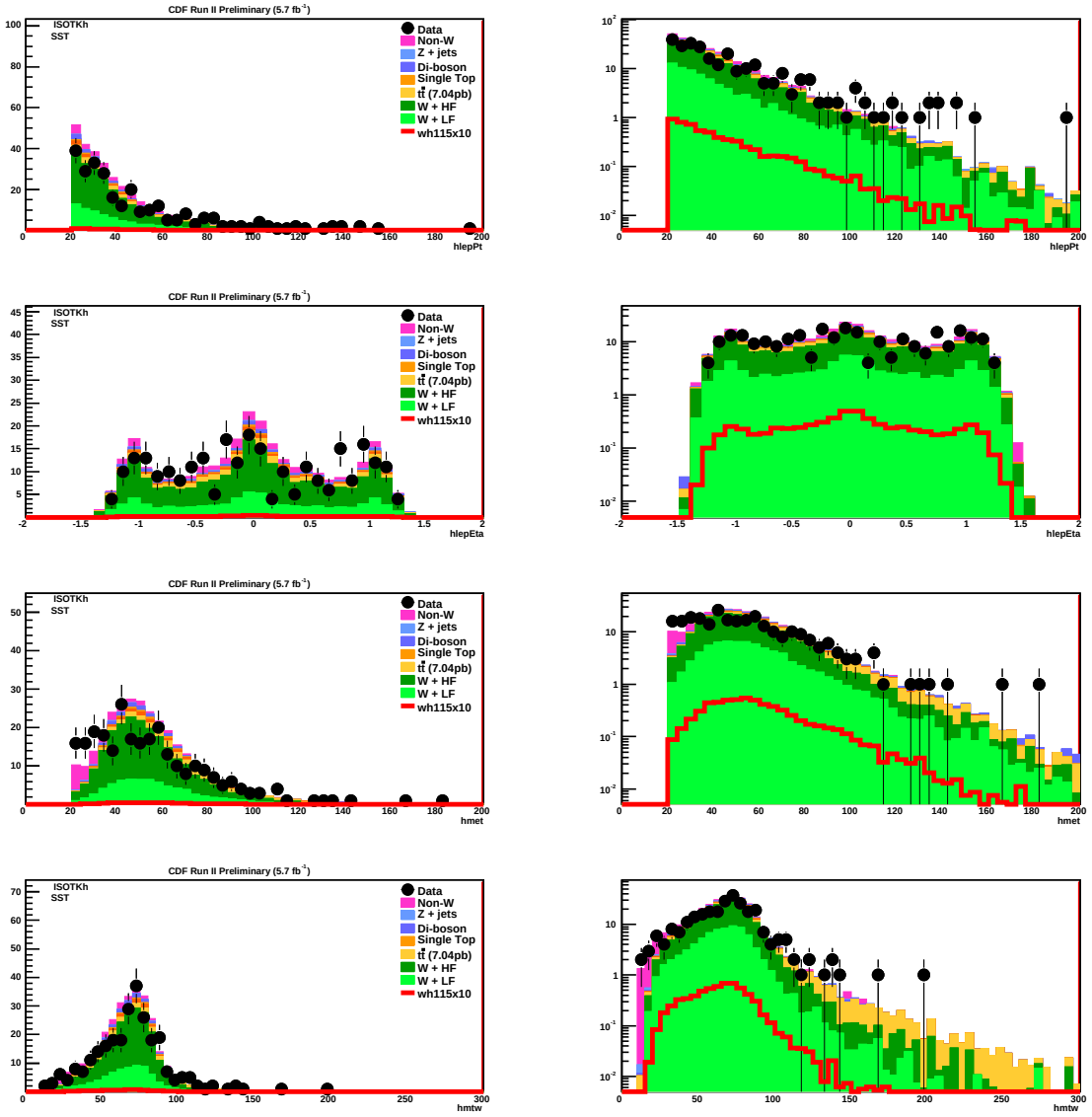

Figure 34: SST kinematic distributions for isolated track p_T, η,$\not\!\!E_T$, and W transverse mass.

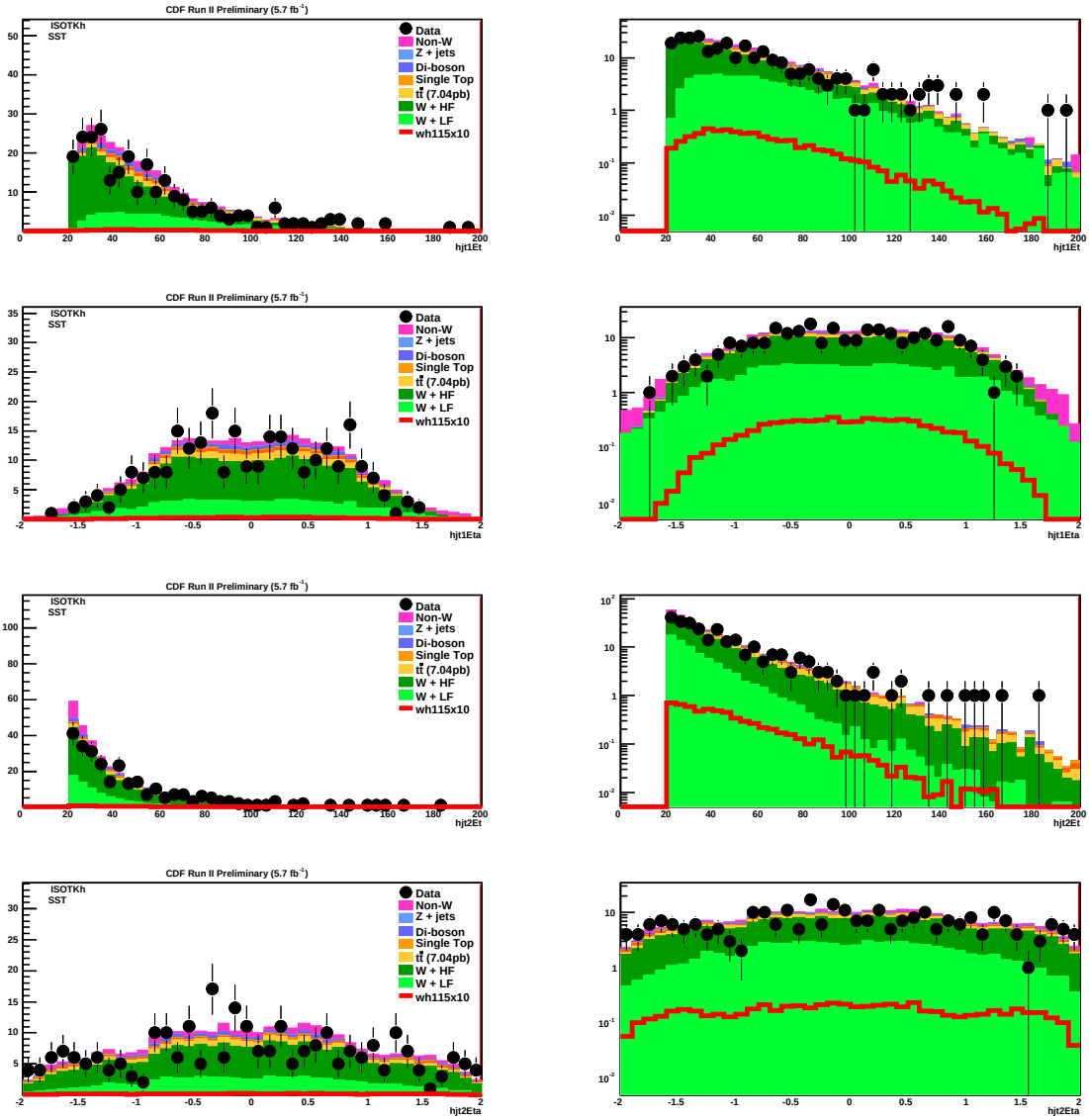

Figure 35: SST kinematic distributions for first jet E_T, η and second jet E_T, η.

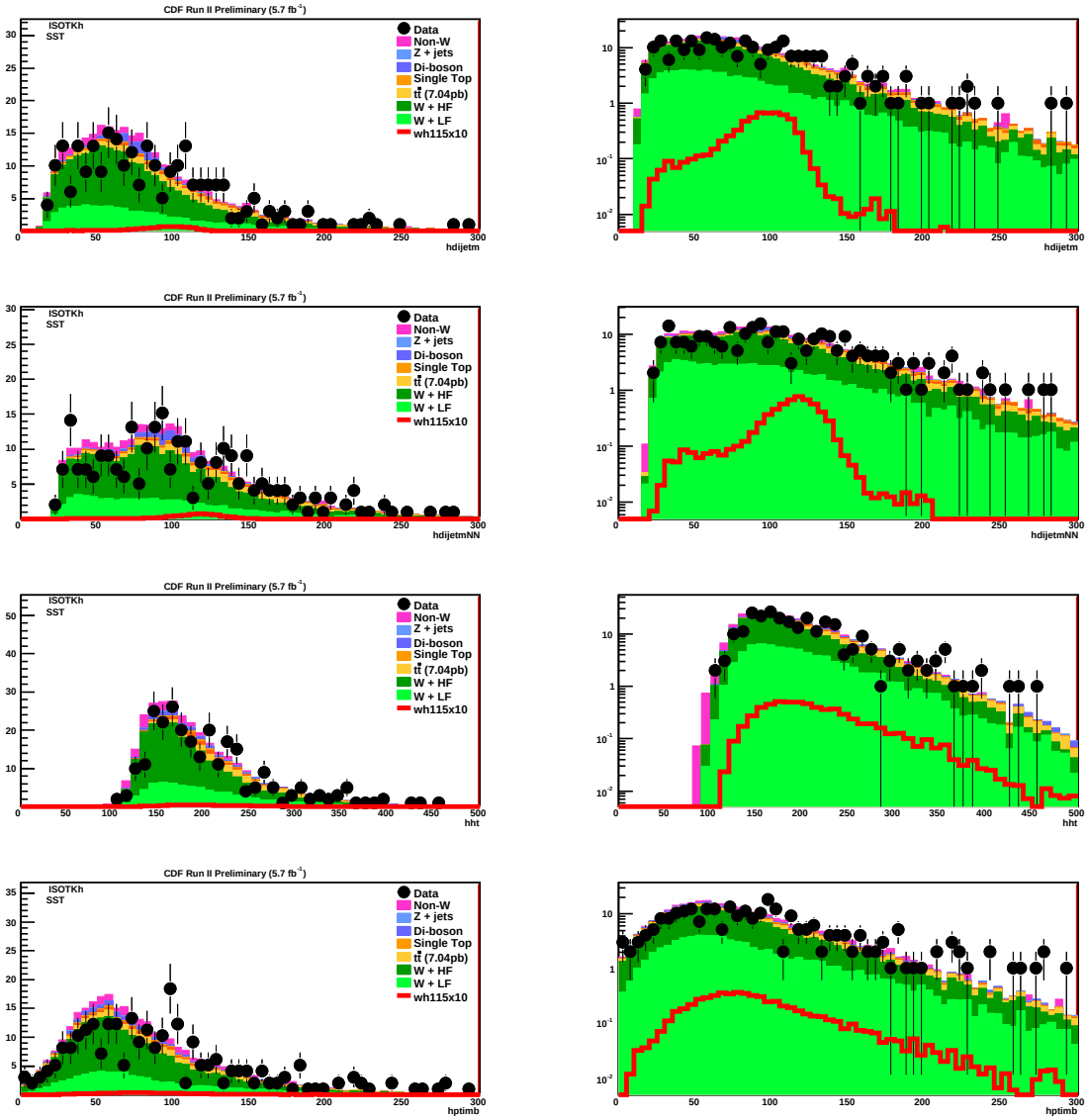

Figure 36: SST kinematic distributions for dijet mass before and after bjet energy correction, H_T, and P_T imbalance.

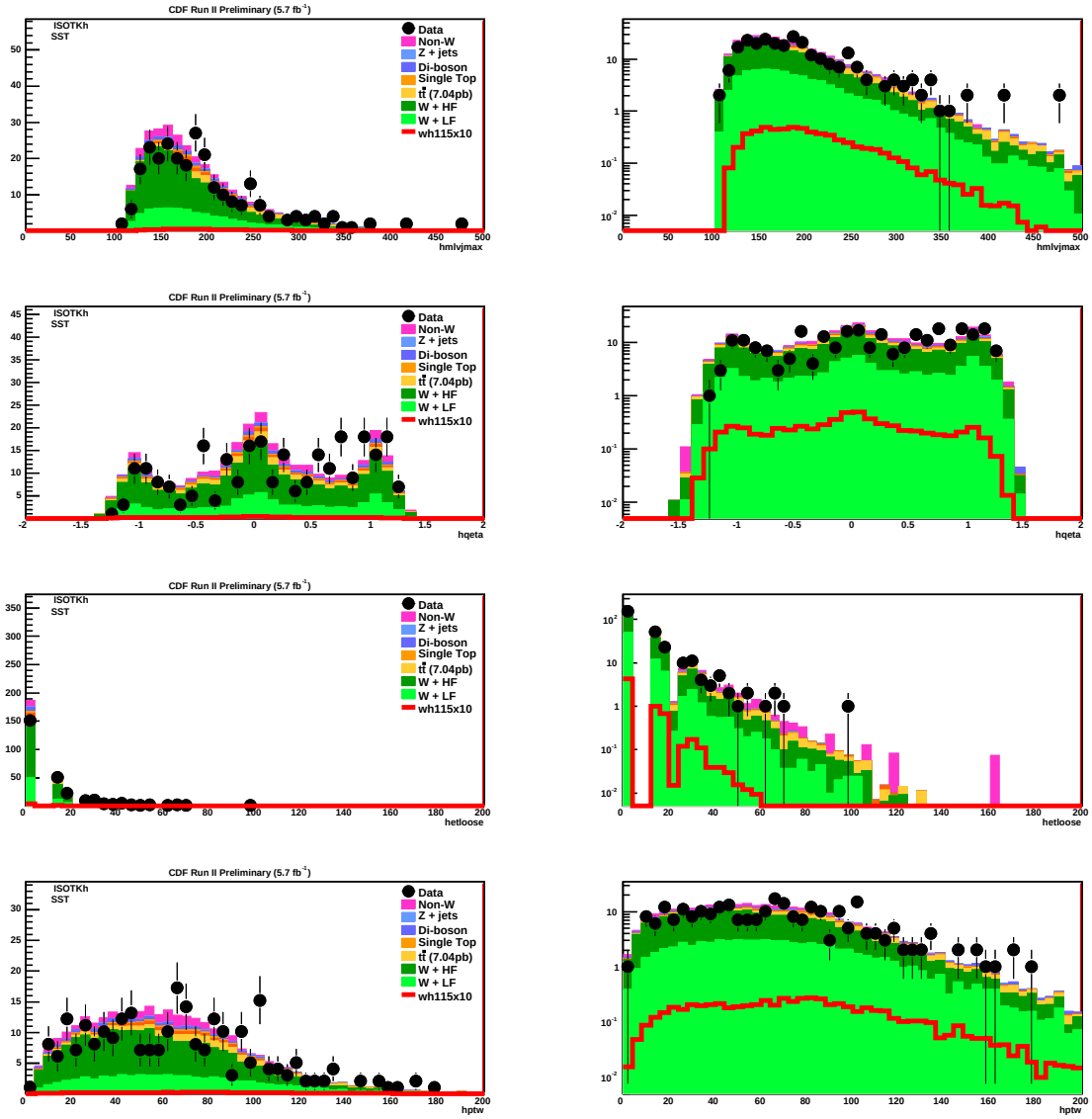

Figure 37: SST kinematic distributions for maximum of lvj mass, $\eta \times Q$, sum loose jet E_T, and P_T of W candidate.

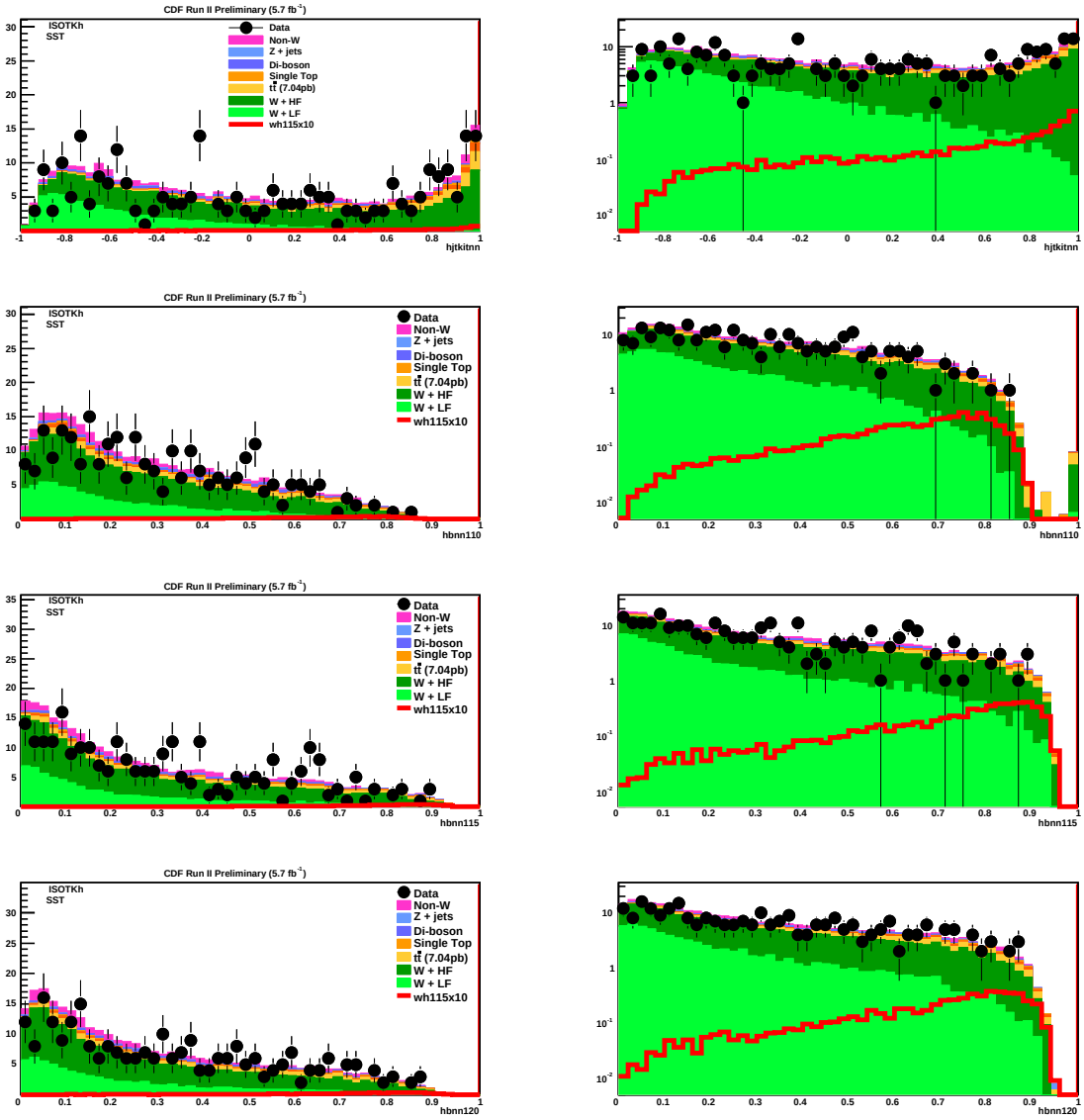

Figure 38: SST kinematic distributions for kitnn and Bnn output corresponds to m_H =110, 115, 120 GeV/c^2 respectively.